Myosin-X is required for integrin activation at filopodia tips

Mitro Miihkinen[1], Max L.B. Grönloh[1,*], Helena Vihinen[2], Eija Jokitalo[2], Benjamin T. Goult[3], Johanna Ivaska[1,4 ✉], and Guillaume Jacquemet[1-5 ✉]

[1]Turku Bioscience Centre, University of Turku and Åbo Akademi University, FI-20520 Turku, Finland
[2]Electron Microscopy Unit, Institute of Biotechnology, University of Helsinki, FI-00790 Helsinki, Finland
[3]School of Biosciences, University of Kent, Canterbury, Kent CT2 7NJ, UK
[4]Department of Biochemistry, University of Turku, FI- 20520, Turku, Finland
[5]Faculty of Science and Engineering, Cell Biology, Åbo Akademi University, FI-20520 Turku, Finland
[*]Current address: Molecular Cell Biology lab, Department of Molecular Cellular Hemostasis, Sanquin Research and Landsteiner Laboratory, 1066 CX Amsterdam, The Netherlands.

Filopodia assemble unique integrin-adhesion complexes as they sense and attach to the surrounding extracellular matrix. Integrin activation is essential for filopodia stability; however, the regulation of integrin activity within filopodia is poorly defined. Using structured illumination and scanning electron microscopy, we observed that active integrin is spatially confined to filopodia tips and inactive integrin localises throughout the filopodia shaft. RNAi depletion of integrin regulators identified FERM domain containing talin and MYO10 as critical regulators of filopodia function. Importantly, deletion of MYO10-FERM ablates the active pool of integrin from filopodia, indicating that MYO10-FERM domain is required for integrin activation but not for integrin transport to filopodia tips. Yet, remarkably, the MYO10-FERM domain binds both α and β integrin tails restricting integrin activation. Swapping MYO10-FERM with talin-FERM leads to an over-activation of integrin receptors in filopodia. Our observations demonstrate a complex regulation of integrin activity, at filopodia tips, via MYO10-FERM domain and challenge the concept of MYO10-dependent integrin transport in filopodia.

Filopodia| integrin activity| adhesion| MYO10| Talin
Correspondence: *johanna.ivaska@utu.fi and guillaume.jacquemet@abo.fi*

Introduction

Filopodia are actin-rich "antenna-like" protrusions that are responsible for constantly probing the cellular environment composed of neighbouring cells and the extracellular matrix (ECM). As such, filopodia contain cell-surface receptors such as integrins, cadherins and growth factor receptors that can interact with, and interpret, a wide variety of extracellular cues (Jacquemet et al., 2015). Filopodia are especially abundant in cells as they migrate in 3D and in vivo where they contribute to efficient directional migration by probing and remodelling the surrounding ECM (Jacquemet et al., 2013, 2017; Paul et al., 2015).

Filopodia have a unique cytoskeleton composed of tightly packed parallel actin filaments with barbed ends oriented towards the filopodium tip (Mattila and Lappalainen, 2008). This organisation allows molecular motors, such as unconventional myosin-X (MYO10), to move towards and accumulate at filopodia tips. By doing so, these molecular motors are thought to transport various proteins, including integrins, along actin filaments to the tips of filopodia

(Jacquemet et al., 2015; Arjonen et al., 2014; Berg and Cheney, 2002; Hirano et al., 2011; Zhang et al., 2004). In particular, MYO10 is known to bind directly to the NPxY motif of the β-integrin cytoplasmic tail via its FERM (protein 4.1R, ezrin, radixin, moesin) domain (Zhang et al., 2004). At filopodia tips, integrins assemble a specific adhesion complex that tethers filopodia to the ECM (Alieva et al., 2019; Jacquemet et al., 2019; Gallop, 2019). In particular, filopodia adhesions contain several adhesions proteins including talin, kindlin and p130Cas but are devoid of the nascent adhesion markers focal adhesion kinase (FAK) and paxillin (Jacquemet et al., 2019). The subsequent maturation of these filopodia adhesions into nascent and focal adhesions can then promote directional cell migration (Hu et al., 2014; Jacquemet et al., 2016, 2019).

Integrin functions are tightly regulated by a conformational switch that modulates ECM binding, often referred to as activation. Integrin extracellular domain conformations can range from a bent to an extended open conformation, where the integrin's ligand affinity increases with stepwise opening (Conway and Jacquemet, 2019; Sun et al., 2019; Askari et al., 2009). For β1 integrin, this unfolding can be viewed using activation-specific antibodies (Byron et al., 2009). Mechanistically, integrin activity can be finely tuned, from within the cell, by multiple proteins that bind to the integrin cytoplasmic tails (Conway and Jacquemet, 2019; Sun et al., 2019; Askari et al., 2009). For instance, talin, a key integrin activator, can bind to the NPxY motif of the β integrin cytoplasmic tail leading to the physical separation of the integrin and β cytoplasmic tails and integrin activation . Kindlin, another critical regulator of integrin activity, also binds to β integrin cytoplasmic tails where it cooperates with talin to induce integrin activation (Sun et al., 2019). While it is clear that integrins and integrin signalling are key regulators of filopodia function (Lagarrigue et al., 2015; Jacquemet et al., 2016, 2019; Gallop, 2019), how integrin activity is regulated within filopodia remains unstudied.

Using super-resolution microscopy, we observed that integrin activation is spatially controlled within filopodia, where active (high affinity) integrin accumulates at filopodia tips, and inactive (unoccupied) integrin localises throughout the filopodia shaft. We demonstrate that integrin activation at

filopodia tips occurs independently of the rest of the cell and is instead locally regulated by talin and MYO10. We report that contrary to previous assumptions, the MYO10-FERM domain is not required to transport integrin to filopodia but is instead required to localise active integrin to filopodia tips. Counterintuitively, we discovered that MYO10-FERM itself is capable of inactivating integrins by binding to both the α and β integrin subunit cytoplasmic tails and presumably cross-linking the heterodimer. Yet, remarkably, swapping MYO10-FERM with talin-FERM rescued filopodia function and integrin activation at filopodia tips, suggesting an unanticipated level of interchangeability between FERM domains in spatially regulating integrin activation in filopodia.

Main text

Active integrins accumulate at filopodia tips. We and others have previously described the formation of integrin-mediated adhesions at filopodia tips and that these structures are required for ECM sensing (Shibue et al., 2012; Jacquemet et al., 2019; Lagarrigue et al., 2015; Alieva et al., 2019; Gallop, 2019). To gain insight into how integrin activity is regulated in filopodia, we first assessed the spatial distribution of high affinity and unoccupied β1 integrin (termed active and inactive integrin for simplicity) in U2-OS cells transiently expressing fluorescently-tagged MYO10 using structured illumination microscopy (SIM) (Fig. 1A and 1B) and scanning electron microscopy (SEM) (Fig. 1C). The average distribution of the β1 integrin species along filopodia was mapped from both the SIM and the SEM images (Fig. 1B and 1C) revealing that active β1 integrins mainly accumulate at filopodia tips (active integrin detected in 68% of filopodia tips). In contrast, inactive β1 integrins are distributed along the entire length of the filopodium. This pattern of integrin localisation was recapitulated in endogenous filopodia, forming in actively spreading cells, and thus is not a specific feature of cells over-expressing MYO10 (Fig. 1D and 1E).

Previous work reported that forces generated by the actomyosin machinery are required for integrin-mediated adhesion at filopodia tips (Alieva et al., 2019). In addition, we observed that filopodia often align to the force generated by focal adhesions (Stubb et al., 2020). Therefore, we investigated whether cellular forces generated by the cell body and transmitted at focal adhesions were responsible for integrin activation at filopodia tips. U2-OS cells expressing fluorescently-tagged MYO10 and adhering to fibronectin were treated with DMSO, a myosin II inhibitor (10 μM blebbistatin) or an established focal adhesion inhibitor (CDK1 inhibitor, 10 μM RO-3306 (Robertson et al., 2015; Jones et al., 2018)). As expected, inhibition of myosin II or CDK1 led to rapid disassembly of focal adhesions (Fig. 1F and S1A). Blebbistatin treatment promoted longer and more numerous filopodia, in line with our earlier report (Stubb et al., 2020), while treatment with the CDK1 inhibitor increased filopodia numbers but not filopodia length (Fig. S1B and S1C). However, no decrease in filopodial integrin activation could be observed when myosin II or CDK1 were inhibited (Fig. 1F and 1G). In contrast, CDK1 inhibition led to an increase in the percentage

of filopodia with active integrin at their tips (Fig. 1H). Altogether these data indicate that integrin activation at filopodia tips is regulated independently of cellular forces and focal adhesions. However, cellular forces are likely required to induce filopodia adhesion maturation into focal adhesions and for efficient ECM sensing (Alieva et al., 2019; Jacquemet et al., 2019).

Inside-out integrin activation in filopodia . The obvious enrichment of active β1 integrin at filopodia tips (Fig. 1) indicates that β1 integrin activation is likely to be spatially regulated by one or multiple components of the filopodium tip complex. We and others have previously reported that several proteins implicated in the regulation of integrin activity, including the integrin activators talins and kindlins as well as the integrin inactivator ICAP-1 (ITGB1BP1), accumulate at filopodia tips where their function remains mostly unknown (Lagarrigue et al., 2015; Jacquemet et al., 2019). In addition, we previously reported that modulation of integrin activity often correlates with increased filopodia numbers and stability (Jacquemet et al., 2016). Therefore, to test the contribution of 10 known integrin activity regulators to filopodia formation, a microscopy-based siRNA screen was performed in U2-OS cells stably expressing MYO10-GFP (Fig. S1D) (Jacquemet et al., 2016). The silencing efficiency of each siRNA was validated by qPCR (Fig. S1E) or western blot (Fig. S1F), and silencing of MYO10 was included as a positive control.Of the ten integrin regulators, only talin (combined TLN1 and TLN2) silencing significantly influenced filopodia numbers. As kindlin-2 (FERMT2) is a major regulator of integrin activity (Theodosiou et al., 2016) and FERMT2 localises to filopodia tips (Jacquemet et al., 2019), we were surprised by the inability of FERMT2 silencing to impact filopodia and therefore we decided to explore this further. Dual silencing of FERMT1 and FERMT2 did not affect filopodia number or dynamics suggesting that kindlins are not directly required to support filopodia formation or adhesion under the conditions tested (Fig. S1G-I). Altogether, our data indicate that, in line with our previous work (Jacquemet et al., 2016), talin and MYO10 are key regulators of filopodia functions. As Rap1 also plays a key role in filopodia functions (Lagarrigue et al., 2015; Jacquemet et al., 2016), future work will aim to unravel if talin is directly activated by Rap1 in filopodia (Gingras et al., 2019; Zhu et al., 2017) or if Riam is also required (Lagarrigue et al., 2015).

The FERM domain of MYO10 is required for integrin activation at filopodia tips. MYO10 directly binds to integrins via its FERM domain (Hirano et al., 2011; Zhang et al., 2004). In this context, MYO10 is thought to actively transport integrins as well as other cargo to filopodia tips. Therefore, we next assessed the contribution of MYO10-FERM domain to the localisation of the various integrin species in filopodia by creating a FERM domain deletion construct (MYO10$^{\Delta F}$) (Fig. 2A). Importantly, we carefully designed this construct by taking into consideration the previously reported MYO10-FERM domain structures (PDB ids: 3pzd and 3au5) (Wei et al., 2011; Hirano et al., 2011). MYO10$^{\Delta F}$ was expressed in
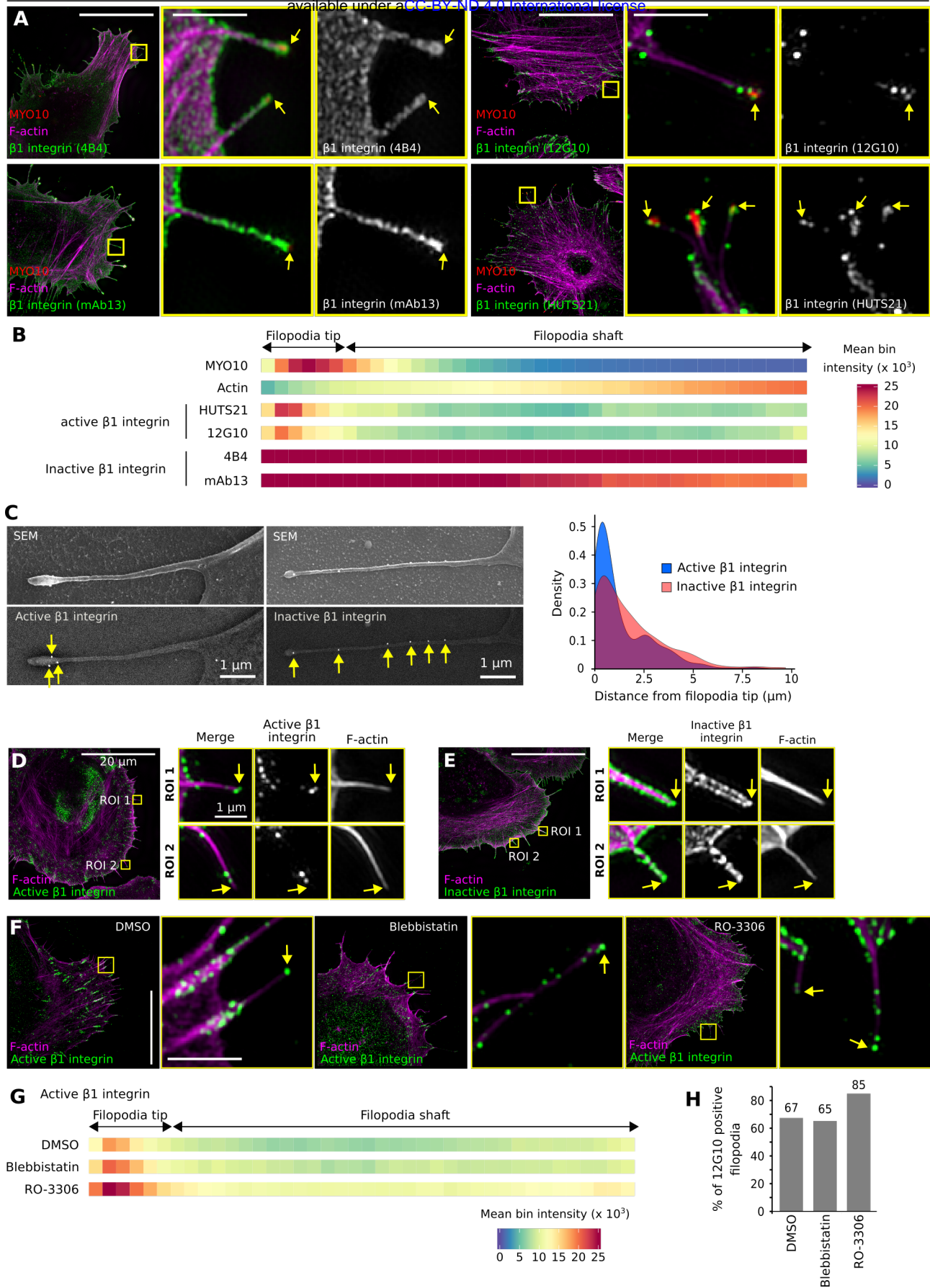
Fig. 1. Active Integrins accumulate at filopodia tips independently of cellular forces A) U2-OS cells expressing mScarlet-MYO10 or EGFP-MYO10 were plated on fibronectin for 2 h, stained for active (high affinity β1 integrin; clone 12G10 and HUTS21) or inactive (unoccupied β1 integrin, clone 4B4 and mAb13) β1 integrin and F-actin, and imaged using structured illumination microscopy (SIM). Representative maximum intensity projections (MIPs) are displayed. The yellow squares highlight regions of interest (ROIs), which are magnified; yellow arrows highlight filopodia tips; scale bars: (main) 20 μm; (inset) 2 μm. **B**) Heatmap highlighting the sub-filopodial localisation of the proteins stained in A based on their intensity profiles (See methods for details, MYO10, n = 623 filopodia; F-actin, n = 623 filopodia; HUTS21, n = 538 filopodia; 12G10, n = 329 filopodia; 4B4, n = 413 filopodia; mAb13, n = 369 filopodia; thee biological repeats). The segments corresponding to the filopodia tip and shaft are indicated.

Fig. 1. (Continued from previous page.) **C)** U2-OS cells were plated on fibronectin for 2 h, stained for active (clone 12G10) or inactive (clone 4B4) β1 integrin and imaged using a scanning electron microscope (SEM). Representative images are displayed. The upper row was acquired using a secondary electron detector (SED) and the lower row using a backscattered electron detector (vCD). The distance of the two β1 integrin pools from the filopodia tip (defined by the gold particles, highlighted by yellow arrows) was measured and the results displayed as a density plot (4B4 staining n = 175 gold particles; 12G10 staining n = 178 gold particles). A bootstrap version of the univariate Kolmogorov-Smirnov test was used for statistical testing. p-value < 0.001. **D-E)** U2-OS cells were plated on fibronectin for 20 min, stained for active (**D**, clone 12G10) or inactive (**E**, clone 4B4) β1 integrin and F-actin, and imaged using SIM. Representative MIPs are displayed. The yellow squares highlight ROIs, which are magnified; yellow arrows highlight filopodia tips; scale bars: (main) 20 μm; (inset) 2 μm. **F-H)** U2-OS cells expressing EGFP-MYO10 were plated on fibronectin for 1 h and treated for 1 h with 10 μM blebbistatin (myosin II inhibitor), 10 μM RO-3306 (CDK1 inhibitor) or DMSO. Cells were stained for active β1 integrin (clone 12G10) and F-actin, and imaged using SIM. **F)** Representative MIPs are displayed. The yellow squares highlight ROIs, which are magnified; yellow arrows highlight filopodia tips; scale bars: (main) 20 μm; (inset) 2 μm. **G)** Heatmap displaying the sub-filopodial localization of active β1 integrin in cells treated with DMSO, blebbistatin or RO-3306 (DMSO, n = 734 filopodia; RO-3306, n = 824 filopodia; blebbistatin, n = 483 filopodia; three biological repeats). **H)** Bar chart highlighting the percentage of filopodia with detectable levels of active β1 integrin in cells treated with DMSO, blebbistatin or RO-3306 (DMSO, n = 734 filopodia; RO-3306, n = 824 filopodia; blebbistatin, n = 483 filopodia; three biological repeats).

U2-OS cells, which express very low levels of endogenous MYO10 (Young et al., 2018; Jacquemet et al., 2016) (Fig. 2B). Deletion of the MYO10-FERM domain led to a small but significant reduction in filopodia number accompanied with a reduction in filopodia length, in line with previous reports (Zhang et al., 2004; Watanabe et al., 2010) (Fig. 2C and 2D). Strikingly, the majority of MYO10$^{\Delta F}$-filopodia (80%) were devoid of active β1 integrins at their tips (Fig. 2E and 2F). However, this lack of active β1 integrin was not due to an absence of β1 integrin in filopodia, as the uniform inactive β1 integrin distribution along the filopodia was unaffected by the MYO10-FERM domain deletion (Fig. 2E and 2F). In line with these results, MYO10$^{\Delta F}$-induced filopodia were unstable and unable to attach to the underlying ECM (Fig. 2G and Video 1). Taken together, these findings demonstrate that MYO10 supports integrin activation at filopodia tips via its FERM domain. However, MYO10-FERM domain is not required to localise and/or accumulate β1 integrin to filopodia (Fig. 2). These findings challenge the model of MYO10-FERM domain acting as a cargo-transporter of integrin to filopodia tips.

MYO10-FERM deletion does not influence the localisation of key filopodia tip components. As MYO10-FERM domain is thought to be the major cargo binding site in MYO10 (Wei et al., 2011), we hypothesized that the lack of integrin activation at the tip of MYO10$^{\Delta F}$ filopodia would be due to the absence of a key integrin activity modulator. We co-expressed six established filopodia tip components (Jacquemet et al., 2019), TLN1, FERMT2, CRK, DIAPH3, BCAR1 and VASP, with either MYO10^{WT} or MYO10$^{\Delta F}$. SIM microscopy revealed that the localization of these proteins was unaffected by MYO10-FERM domain deletion (Fig. S2). Interestingly, VASP has been previously described as a MYO10-FERM cargo but its localisation at filopodia tips was clearly un-affected by MYO10-FERM deletion (Young et al., 2018; Tokuo and Ikebe, 2004; Lin et al., 2013). Altogether, our results demonstrate that the recruitment of key filopodia tip proteins is independent of MYO10-FERM domain and suggest that MYO10-FERM may regulate integrin activity via another mechanism than cargo transport.

MYO10-FERM domain alone inactivates integrin. The talin-FERM domain is necessary and sufficient to activate integrins (Anthis et al., 2009; Lilja et al., 2017), and the MYO10-FERM domain is required to activate integrin at filopodia tips (Fig 2). Superimposition of the talin and MYO10-FERM domain revealed that both FERM domains adopt a similar fold, within the talin sub-domains that bind to the β integrin tail (talin F2 and F3). While the site where MYO10-FERM binds to the β integrin tail remains unknown, this structural align-

ment suggests that talin-FERM and MYO10-FERM may operate in a similar fashion (Fig. 3A). To assess whether MYO10-FERM modulates integrin activity, we employed a flow cytometric assay to measure active cell-surface integrins relative to total cell-surface integrins (Lilja et al., 2017) (Fig. 3B-D). As expected overexpression of the talin-FERM domain significantly increased integrin activity (Fig. 3B). In contrast, overexpression of the MYO10-FERM domain led to a small but highly reproducible decrease in integrin activity in CHO and U2-OS cells (Fig. 3B-C). A similar decrease in integrin activity could also be measured when full-length MYO10 was overexpressed in U2-OS cells (Fig. 3C). Conversely, silencing of MYO10 in MDA-MB-231 cells, where mutant p53 drives high endogenous MYO10 levels (Arjonen et al., 2014), increased integrin activity. Reintroduction of full-length MYO10 reversed the increased integrin activity in MYO10-silenced cells (Fig. 3D and S3A). Integrin activity levels have an impact on cellular functions, including cell adhesion and spreading (Lilja et al., 2017). Consistent with decreased integrin activation, MYO10-FERM expression attenuated cell adhesion/spreading on fibronectin over time as measured with the xCELLigence apparatus or by measuring cell spreading area (Fig. 3E-G) (Hamidi et al., 2017). Altogether our data indicate, unexpectedly, that even though MYO10-FERM domain is necessary for spatially restricted integrin activation at filopodia tips, MYO10-FERM domain is capable of inactivating integrins.

MYO10-FERM domain binds to both α and β integrin tails . Given the unexpected ability of MYO10-FERM domain to inactivate integrins (Fig. 3), we next investigated MYO10-FERM and talin-FERM interaction with integrin cytoplasmic tails. Recombinant His-tagged MYO10 and talin-FERM domains were expressed in bacteria, purified (Fig S3B), and their binding affinity to integrin α and β tails was measured using microscale thermophoresis (Fig. 4A and Fig. 4B; see methods for details) (Jerabek-Willemsen et al., 2014). As expected, the FERM domain of talin bound to the β1 and β5 integrin tails (measured affinities of 4.7 μM and 12 μM, respectively) but not to the α integrin tails (Goult et al., 2009). In contrast, the MYO10-FERM interacted with all the α and β integrin-tails tested with affinities ranging from 4 to 25 μM (Fig. 4A and Fig. 4B). This result was surprising as we had not expected MYO10-FERM to bind to α integrin-tails. A shared feature in α-integrin tails (including α5 and α2 integrin) is the highly conserved membrane-proximal GFFKR motif. Importantly, mutation of this GFFKR motif in the α2-integrin tail (FF/AA mutation, named ITGA2^{GAAKR}) abolished the binding of recombinant MYO10-FERM in vitro (Fig. 4C), indicating that MYO10 interaction with α-subunit
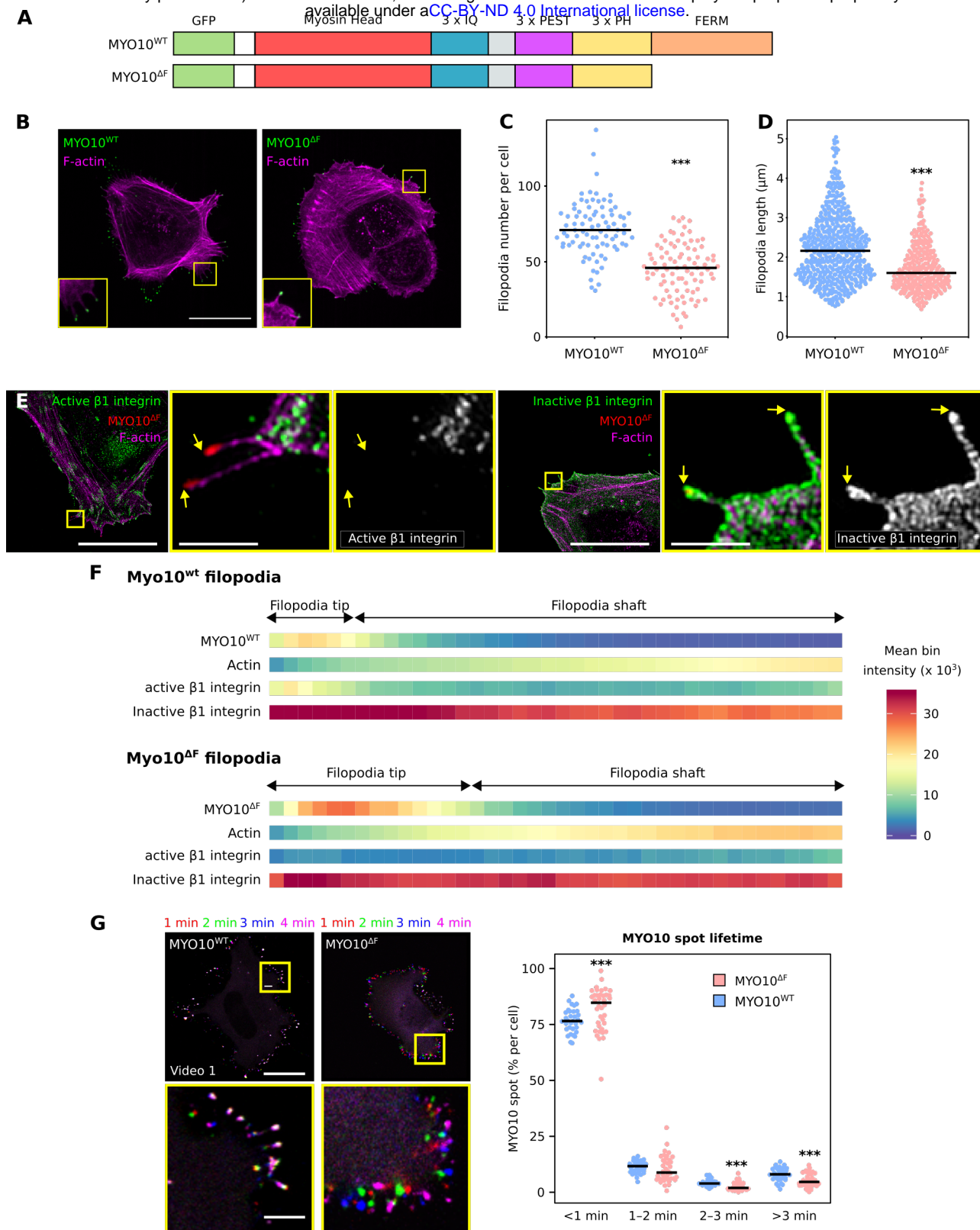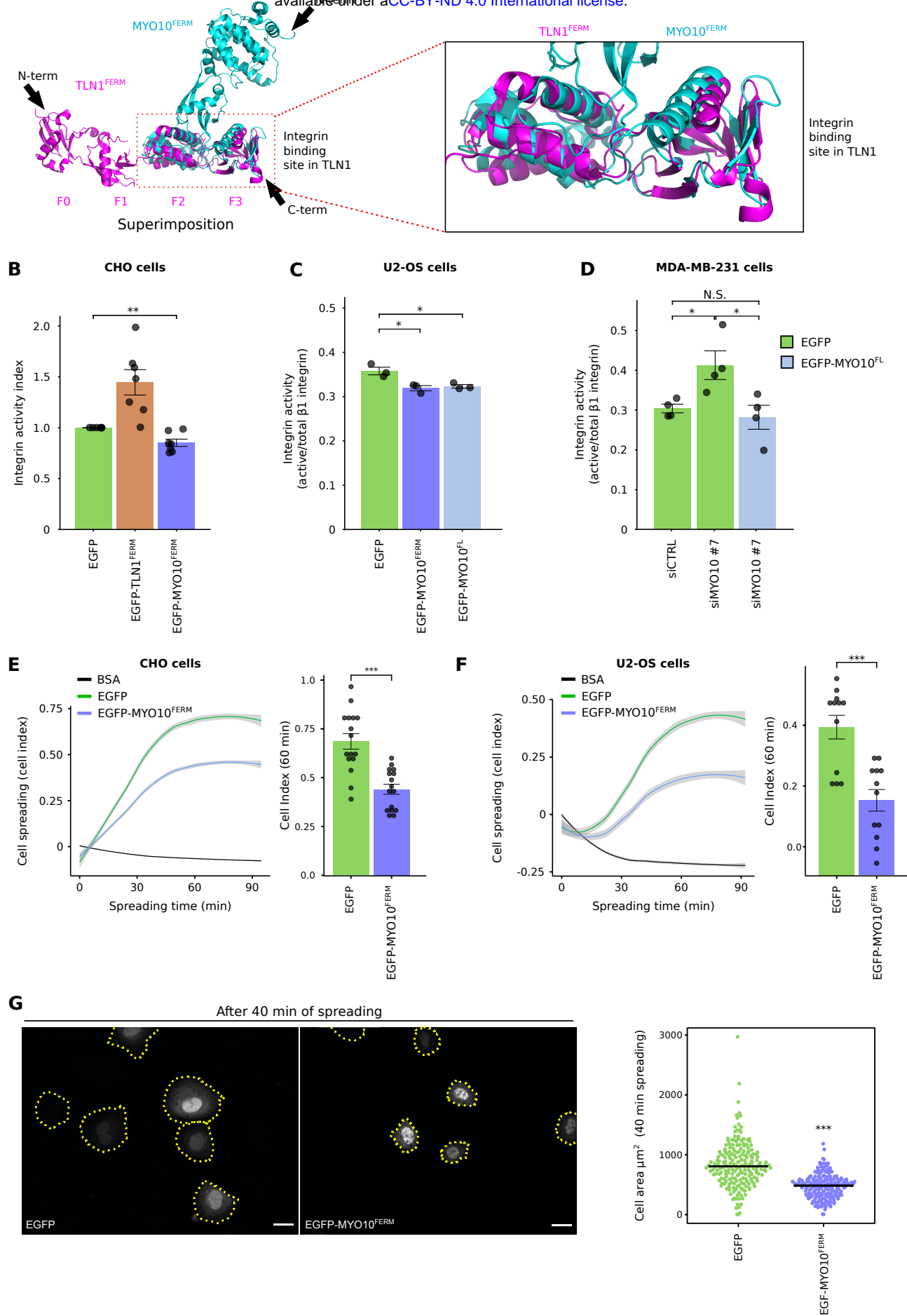
Miihkinen *et al.* | Integrin activation at filopodia tips

Fig. 2. MYO10-FERM domain is required for integrin activation in filopodia. A) Cartoon illustrating the EGFP-MYO10^{WT} and EGFP-MYO10$^{\Delta F}$ constructs. **B-C**) U2-OS cells transiently expressing EGFP-MYO10^{WT} or EGFP-MYO10$^{\Delta F}$ were plated on fibronectin for 2 h, fixed and imaged using a spinning-disk confocal microscope. **B**) Representative MIPs are displayed. Scale bar: 25 µm. **C**) The number of MYO10-positive filopodia per cell was then quantified (n > 85 cells, three biological repeats; *** p-value <0.001). **D**) Quantification of filopodia length in U2-OS cells transiently expressing EGFP-MYO10^{WT} or EGFP-MYO10$^{\Delta F}$ from SIM images (EGFP-MYO10^{WT}, n = 512 filopodia; EGFP-MYO10$^{\Delta F}$, n = 283 filopodia; three biological repeats; *** p value = <0.001). **E**) U2-OS cells expressing EGFP-MYO10$^{\Delta F}$ were plated on fibronectin for 2 h, stained for active (clone 12G10) or inactive (clone 4B4) β1 integrin and F-actin, and imaged using SIM. Representative MIPs are displayed. The yellow squares highlight ROIs, which are magnified; yellow arrows highlight filopodia tips; scale bars: (main) 20 µm; (inset) 2 µm. **F**) Heatmap highlighting the sub-filopodial localisation of the proteins stained in (**E**) generated from their intensity profiles measured within filopodia (EGFP-MYO10^{WT}, n = 512 filopodia; EGFP-MYO10$^{\Delta F}$, n = 283 filopodia; three biological repeats). **G**) U2-OS cells expressing EGP-MYO10^{WT} or EGFP-MYO10$^{\Delta F}$ were plated on fibronectin and imaged live using an Airyscan confocal microscope (1 picture every 5 s over 20 min; scale bar = 25 µm; Video 1). For each condition, MYO10-positive particles were automatically tracked, and MYO10 spot lifetime (calculated as a percentage of the total number of filopodia generated per cell) was plotted and displayed as boxplots (see Methods for details; three biological repeats; EGP-MYO10^{WT}, n= 33 cells; EGFP-MYO10$^{\Delta F}$, n= 38 cells, *** p-value < 0.006). For all panels, p-values were determined using a randomization test.

Fig. 3. MYO10-FERM domain inhibits integrin activity. A) Visualisation of the structure of MYO10-FERM (PDB: 3PZD; (Wei et al., 2011)) and TLN1-FERM (PDB: 3IVF, (Elliott et al., 2010)) domains using PyMOL. The black arrows indicate the protein orientation from N to C terminal. The two FERM domains were superimposed to highlight their structural homology and differences. The integrin binding region on the talin-FERM domain is highlighted and magnified.

Miihkinen *et al.* | Integrin activation at filopodia tips

Fig. 3. (Continued from previous page.) **B)** CHO cells expressing EGFP or C-terminal FERM domains of TLN1 (EGFP-TLN1^{FERM}) or MYO10 (EGFP-MYO10^{FERM}) were either incubated with an Alexa647- labelled fibronectin fragment (FN7–10) and fixed, or fixed directly and stained with a (total) anti-ITGA5 antibody (clone PB1). Samples were then analysed by FACS. The integrin activity index was calculated using the fibronectin and the ITGA5 signals as described in the Methods. Results are displayed as bar charts where the individual experiments are highlighted as dots, and error bars represent standard error of the mean (** p-value = 0.0062, n = 7 of biological repeats). The p-value was determined using a one-sample t-test. **C)** U2-OS or MDA-MB-231 cells transiently expressing various EGFP constructs (as indicated), were fixed and stained for active (clone 9EG7) or total β1 integrin (clone P5D2). Staining intensity was recorded by flow cytometry and integrin activation was assessed as a ratio between active and total integrin (9EG7/P5D2 ratio). Error bars indicate standard error of the mean (* p-value < 0.05; **C**, n = 5 biological repeats; **D**, n = 4 biological repeats). The p-values were determined using a Student's two-tailed t-test. **D)** MDA-MB-231 cells, previously silenced for MYO10 (using an siRNA targeting the 3' UTR of MYO10 mRNA) and expressing EGFP or EGFP-MYO10, were fixed and stained for active (clone 9EG7) or total β1 integrin (clone P5D2). Staining intensity was recorded by flow cytometry and integrin activation was assessed as a ratio between active and total integrin (9EG7/P5D2 ratio). Error bars indicate standard error of the mean (* p-value < 0.05; n = 4 biological repeats). The p-value was determined using a Student's two-tailed t-test. **E-F)** CHO or U2-OS cells transiently expressing EGFP or EGFP-MYO10^{FERM} were left to adhere on fibronectin and their spreading was monitored over time using the xCELLigence system. The cell index over time is displayed, grey areas indicate the 95% confidence intervals. The cell index at 60 min is also displayed as a bar chart (error bars indicate the standard error of the mean, *** p-value < 0.001, n = 4 biological repeats (CHO), n = 3 (U2-OS)). The p-value in bar charts was determined using a Student's two-tailed t-test. **G)** U2-OS cells transiently expressing EGFP or EGFP-MYO10^{FERM} were seeded on fibronectin and allowed to spread for 40 min prior to fixation. Samples were imaged using a confocal microscope and the cell area measured using Fiji (*** p-value < 0.001; EGFP, 208 cells; EGFP-MYO10^{FERM}, 188 cells; n = 3 biological repeats). The p-values were determined using a randomization test. Scale bars are 16 μm.

cytoplasmic tails requires an intact GFFKR-motif. Endogenous MYO10 interacted with both β1 and α2 integrin peptides (Fig. 4D), whereas the clathrin adaptor AP2μ, a known α2 integrin tail binder (De Franceschi et al., 2016), only interacted with the α2 integrin tail (Fig. 4D). Furthermore, the ITGA2^{GAAKR} peptide was defective in interacting with full-length MYO10 (Fig. 4E), but AP2μ recruitment was unaffected (AP2μ binds to a separate motif in the α2-tail) (Fig. 4E). Together, these experiments demonstrate that MYO10 binds to integrin β-tails, in line with previous reports (Zhang et al., 2004; Hirano et al., 2011), and reveal a previously unknown interaction between MYO10-FERM and the GFFKR motif in integrin α tails.

To test the relevance of the MYO10–α-integrin tail interaction in filopodia induction, we expressed full-length ITGA2^{WT} and ITGA2^{GAAKR} in CHO cells (lack endogenous collagen-binding integrins) and investigated MYO10 filopodia formation on collagen I (Fig. 4F). ITGA2^{GAAKR} localises to the plasma membrane and is expressed at similar levels to wild-type in CHO cells (Alanko et al., 2015). Interestingly, the number of filopodia was significantly lower in cells expressing the mutant integrin, indicating that the GFFKR motif in the ITGA2 tail strongly contributes to filopodia formation.

A key step in integrin activation is talin-mediated separation of the α/β tails (Sun et al., 2019; Askari et al., 2009). The ability of MYO10 to bind to both α and β integrin tails, led us to hypothesize that MYO10 could inactivate integrins by promoting an inter-αβ-clasp where both integrin tails are forced together in close proximity (Liu et al., 2015). To assess integrin tail crosslinking, we generated β1 and α2 integrin cytoplasmic tail constructs tagged with an N-terminal membrane targeting sequence (CAAX) and a C-terminal fluorescent protein (mTurquoise2 or YPet). These constructs were expressed in cells and Förster resonance energy transfer (FRET) between mTurquoise2 or YPet was estimated in cells using flow cytometry (Fig. 4G). We found that the expression of mCherry-MYO10-FERM appeared to increase FRET between the two constructs compared to cells expressing mCherry alone (Fig. 4H) and that this increase in FRET was dependent on an intact GFFKR motif in the α2-integrin tail (Fig. 4I). Together these data suggest that the MYO10-FERM domain may be able to inactivate integrins through cross-linking of the two integrin tails. However, the mechanistic details remain to be fully elucidated.

MYO10-FERM domain fine-tunes integrin activity at filopodia tips. To further investigate the contribution of MYO10-FERM in regulating integrin activity in filopodia, we created a chimaera construct, where the FERM domain from MYO10 was replaced by the one from TLN1 (MYO10^{TF}) (Fig. 5A). Cells expressing MYO10^{TF} generated filopodia to nearly the same extent as cells expressing MYO10^{WT} (Fig. 5B). In addition, in a small proportion of cells (below 1%), MYO10^{TF} also localised to enlarged structures connected to stress fibres and reminiscent of focal adhesions (Fig. 5C). The length and the dynamics of MYO10^{TF} filopodia were comparable to filopodia generated by MYO10^{WT} (Fig. 5D-F) and active β1 integrin accumulated at the tips of MYO10^{TF} filopodia (Fig. 5G and 5H). These results indicate that the talin-FERM domain can almost fully rescue the deletion of the MYO10-FERM domain and that the chimeric MYO10^{TF} is functional in filopodia induction in cells. However, MYO10^{TF} filopodia were more likely to have active β1 integrin positive tips, indicating that the talin-FERM domain may facilitate β1 integrin activation in filopodia compared to the MYO10^{WT} filopodia (Fig. 5I). Interestingly, silencing of TLN1 and TLN2 still impeded MYO10^{TF} filopodia formation indicating that talin-FERM fused to the MYO10 motor is not sufficient to substitute for the lack of endogenous full-length talin (Fig. S3C and D).

Altogether, our data indicate that an integrin-binding FERM domain coupled to a Myosin motor is required to activate integrin at filopodia tips (Fig. 2 and 5). We also found that the nature of this FERM domain, whether it is capable of activating or inactivating integrin, then contributes to fine-tuning integrin activation at filopodia tips (Fig. 5). Interestingly, other FERM domain containing myosins, including MYO7 and MYO15, also localise to filopodia tips (Jacquemet et al., 2019) where their roles are mostly unknown. Future work will examine the contribution of these unconventional myosins to filopodia functions. In particular, we identify here that MYO10-FERM domain inhibits integrin activation, possibly through cross-linking integrin α- and β-cytoplasmic tails together (Fig. 3 and 4) in a similar fashion to the integrin inactivator protein FLNA (Liu et al., 2015). However, the exact mechanism by which MYO10-FERM inactivates integrins, as well as the biological significance of this finding, remains to be fully elucidated.

Our data indicate that both MYO10 and talin are required to activate integrins in a spatially controlled manner at filopodia tips. Interestingly, live-cell imaging revealed that, in filopodia, talin and MYO10 always co-localise (Jacquemet
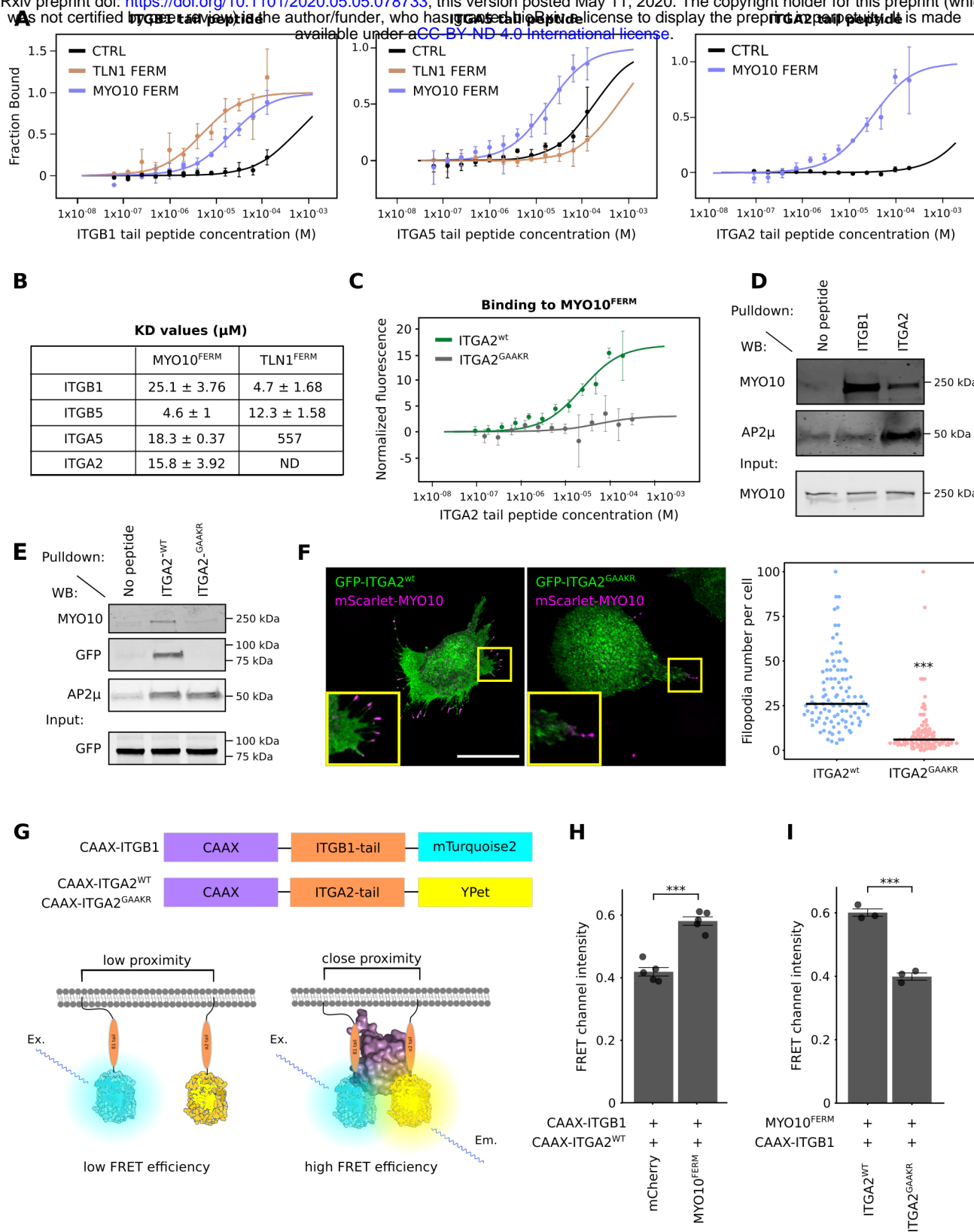
Fig. 4. MYO10 binds to both α and β integrin tails. A) Recombinant 6xHis-tagged FERM domains from TLN1 (TLN1^FERM) and MYO10 (MYO10^FERM) and a 6xHis peptide (CTRL) were labelled and their binding to integrin tails was recorded using microscale thermophoresis. In these experiments, 20 nM of labelled FERM was used while the integrin tail peptides were used at increasing concentration. Graphs were generated by pooling together 3 independent experiments (see Methods for details). **B)** Table showing the Kd values obtained when measuring the binding, using microscale thermophoresis, of TLN1^FERM and MYO10^FERM to the indicated integrin tail peptides. For each condition, data from 3 independent experiments were pooled together to obtain Kd values. **C)** Recombinant MYO10-FERM domain (MYO10^FERM) was labelled and its binding to the intracellular tails of wild type ITGA2 (ITGA2^WT) or of ITGA2 mutated on the GFFKR consensus site (ITGA2^GAAKR) was recorded using microscale thermophoresis. In these experiments, 20 nM of MYO10-FERM was used while the integrin tail peptides were used at increasing concentration. Graphs were generated by pooling together 3 independent experiments (see methods for details). **D)** Integrin tail pull-downs were performed from U2-OS cell lysates using magnetic beads. The recruitment of MYO10 and AP2μ was then analysed by western blot (n = 3 biological experiments). A representative western blot is displayed. **E)** Integrin tail pull-downs were performed from cell lysate generated from U2-OS cells stably expressing EGFP-MYO10^FERM. The recruitment of endogenous MYO10, EGFP-MYO10^FERM and AP2μ was then analysed by western blot (n = 3 biological experiments). A representative western blot is displayed. **F)** CHO cells transiently expressing mScarlet-MYO10 and full length GFP-ITGA2^WT or GFP-ITGA2^GAAKR were plated on collagen I for 2 h, fixed and imaged using a spinning-disk confocal microscope. Representative MIPs are displayed. Scale bar: 25 μm. The number of MYO10-positive filopodia per cell was then quantified (n > 107 cells, four biological repeats; *** p-value < 0.001). P-values were determined using a randomization test. **G)** Cartoons illustrating the two constructs used to measure α and β integrin tail cross-linking in cells using FRET.

Miihkinen *et al.* | Integrin activation at filopodia tips

Fig. 4. (Continued from previous page.) **H)** U2-OS cells transiently expressing the CAAX-ITGB1 and CAAX-ITGA2^{WT} probes, as well as mCherry or mCherry-MYO10^{FERM}, were analysed by flow cytometry. FRET between the CAAX-ITGB1 and CAAX-ITGA2^{WT} probes was estimated as detailed in the Methods. Results are displayed as bar charts where the individual experiments are visible as dots (error bars indicate the standard error of the mean, *** p-value = 3.2*10-5, n = 5 biological repeats). P-values were determined using two-tailed Student's t-test. **I)** U2-OS cells transiently expressing the CAAX-ITGB1 and mCherry-MYO10^{FERM} constructs as well as CAAX-ITGA2^{WT} or CAAX-ITGA2^{GAAKR} probes were analysed by flow cytometry. FRET between the CAAX-ITGB1 and CAAX-ITGA2 probes was estimated as detailed in the methods. Results are displayed as bar charts where the individual experiments are visible as dots (error bars indicate the standard error of mean, *** p = 0.00025, n = 3 biological repeats). The p-values were determined using the two-tailed Student's t-test.

et al., 2019). As the small GTPase Rap1 localises to filopodia and is required to support filopodia functions (Jacquemet et al., 2016; Lagarrigue et al., 2015), a plausible mechanism would be that, upon filopodia initiation, talin is kept in an auto-inhibited conformation in filopodia tips. Once activated by Rap1 (directly or indirectly), talin auto-inhibition is released, and talin associates with and activates integrins, triggering adhesion. Why MYO10-FERM domain is required to activate integrin remains unknown. However, we speculate that, owing to its motor domain, MYO10 allows integrins to resist the strong actin retrograde flow, present in filopodia (Bornschlögl et al., 2013), long enough for the auto-inhibition of talin to be released, and for the integrin to be handed over to, and activated by talin. In this model, MYO10 could act as a sink and interact with integrins only at filopodia tips (He et al., 2017).

The precise mechanism(s) regulating the handing over of integrin from MYO10 to talin remains to be elucidated, but one possibility is that talin-FERM outcompetes MYO10-FERM. Indeed, our in vitro experiments indicate that talin-FERM has, in solution, a higher affinity for integrin β-tail compared to MYO10-FERM (Fig. 4). In addition, talin affinity for β integrin tails will be even stronger in cells due to the presence of negatively charged membrane phosphoinositides (Chinthalapudi et al., 2018; Franceschi et al., 2019), which are known to accumulate at filopodia tips (Jacquemet et al., 2019). Collectively, these findings suggest that a motor-coupled integrin-binding FERM domain is a core requirement for integrin activation in filopodia tips. Interestingly, even though the FERM domains of talin and MYO10 have interchangeable functionality in filopodia, MYO10-FERM domain specifically fine-tunes integrin activation in filopodia.

Material and methods.

Cells. U2-OS (human osteosarcoma cells) and MDA-MB-231 (triple-negative human breast adenocarcinoma) cells were grown in DMEM (Dulbecco's Modified Eagle's Medium with HEPES modification; Sigma, D1152) supplemented with 10% fetal bovine serum (FCS) (Biowest, S1860). U2-OS cells were purchased from DSMZ (Leibniz Institute DSMZ-German Collection of Microorganisms and Cell Cultures, Braunschweig DE, ACC 785). CHO cells were cultured in alpha-MEM, supplemented with 5% FCS and L-glutamine. U2-OS, MDA-MB-231 and CHO cells were transfected using Lipofectamine 3000 and the P3000^{TM} Enhancer Reagent (Thermo Fisher Scientific) according to the manufacturer's instructions. The U2-OS MYO10-GFP lines were generated by transfecting U2-OS cells using lipofectamine 3000 (ThermoFisher Scientific), selected using Geneticin (ThermoFisher Scientific; 400 µg.ml^{-1} final concentration) and sorted for green fluorescence using a fluorescence-assisted cell sorter (FACS). All cell lines tested negative for mycoplasma.

Plasmids. EGFP-MYO10 was a gift from Emanuel Strehler (Addgene plasmid 47608) (Bennett et al., 2007). CRK-GFP was a gift from Ken Yamada (Addgene plasmid 50730). DIAPH3-GFP and VASP-GFP were gifts from Michael Davidson (Addgene plasmids 54158 and 54297, respectively). BCAR1-GFP was a gift from Daniel Rösel (Charles University in Prague, Czech Republic) (Braniš et al., 2017). FERMT2-GFP was a gift from Maddy Parsons (King's College London, UK). The following constructs were described previously: GFP-ITGA2 and GFP-ITGA2^{GAAKR} (Pellinen et al., 2006), mScarlet-MYO10 (Jacquemet et al., 2019), GFP-TLN1 (Kopp et al., 2010), GFP-TLN1^{FERM} and His-TLN1^{FERM} (Goult et al., 2010).

The construct encoding the EGFP-tagged MYO10-FERM domain (EGFP-MYO10^{FERM}) was designed using the boundaries from the MYO10-FERM crystal structure (Wei et al., 2011). The MYO10 coding region 1480-2053 was amplified by PCR (primers: 5'-ATT AGA GAA TTC AAC CCG GTG GTC CAG TGC-3', 5'-ATT AGA GGT ACC TCA CCT GGA GCT GCC CTG-3') and the resulting PCR products were ligated into pEGFP-C1 using the EcoRI and KpnI restriction sites.

To generate the His-tagged MYO10^{FERM} plasmid, the MYO10-FERM domain (boundaries 1504-2058 in MYO10) was amplified by PCR (primers: 5'-ATT AGA GCG GCC GCA CCG ATC GAC ACC CCC AC, 5'-ATT AG AGA ATT CTC ACC TGG AGC TGC CCT G) and introduced in pET151 using the NotI and EcoRI restriction sites.

The MYO10 MyTH/FERM deletion construct (EGFP-MYO10$^{\Delta F}$) was generated by introducing a premature stop codon in full length EGFP-MYO10 (boundaries 1-1512 in MYO10) using a gene block (IDT). The gene block was inserted in EGFP-MYO10 using the PvuI and XbaI restriction sites.

The mScarlet-I-MYO10$^{\Delta F}$ construct was created from EGFP-MYO10$^{\Delta F}$ by swapping the fluorescent tag. The mScarlet-I (Bindels et al., 2017) coding sequence, acquired as a gene block (IDT), was inserted in EGFP-MYO10$^{\Delta F}$ using the NheI and KpnI restriction sites.

The MYO10/TLN1 chimaera construct (EGFP-MYO10^{TF}) was generated by swapping the MYO10-FERM domain (boundaries 1504-2056 in MYO10) with the TLN1 FERM domain (boundaries 1-398 in TLN1) using a gene block (IDT). The gene block was inserted in EGFP-MYO10 using the PvuI and XbaI restriction sites.

The CAAX-ITGB1, CAAX-ITGA2 and CAAX-ITGA2^{GAAKR} constructs were generated by using the Gateway cloning system. Gene blocks containing the CAAX sequence, the integrin cytoplasmic tail and mTurquoise2 or YPet were inserted into the Gateway entry backbone pENTR2b using the XhoI/KpnI restriction sites. The open reading frame was then transferred into the Gateway expression vector pEF.DEST51 using a standard LR reaction (ThermoFisher Scientific, 11791020). All the constructs generated

in this study are in the process to be deposited to Addgene.

Antibodies and other reagents. Monoclonal antibodies recognising the extended conformation of β1 integrin (high affinity for ligand, termed 'active') were mouse anti-human β1 integrin 12G10 (generated in house from a hybridoma), mouse anti-human β1 integrin HUTS21 (556048, BD Biosciences) and rat anti-human β1 integrin 9EG7 (BD Biosciences, 553715). Monoclonal antibodies recognising the closed conformation of β1 integrin (unoccupied β1 integrin, termed 'inactive') were mouse anti-human β1 integrin 4B4 (Beckman Coulter, 6603113) and rat anti-human β1 integrin mAb13 (generated in house from a hybridoma). The monoclonal antibody recognising all β1 integrin species was mouse anti-human β1 integrin P5D2 (Developmental studies hybridoma bank). Other mouse monoclonal antibodies used in this study were raised against hamster α5 integrin (clone PB1, Developmental studies hybridoma bank), TLN1 (clone 97H6, Novus Biologicals NBP2-50320), TLN2 (clone 68E7, Novus Biologicals NBP2-50322), β-actin (Clone AC-15, Sigma, Cat. No. A1978) and PAX (Clone 349, BD Biosciences, 610051). The rabbit monoclonal antibody used was raised against AP2γ (Novus Biological, EP2695Y). Rabbit polyclonal antibodies used were raised against GFP (Abcam Ab290), MYO10 (Novus Biologicals, 22430002; 1:1000 for WB) and kindlin-1 (recognise kindlin 1 and 2, Abcam, ab68041). Small molecule inhibitors used were RO-3306 (CDK1 inhibitor, Sigma SML0569) and blebbistatin (Stemcell technologies 72402). The bovine plasma fibronectin was purchased from Merck (341631) and collagen I was purchased from Sigma (C8919-20ML).

siRNA-mediated gene silencing. The expression of proteins of interest was suppressed using 83 nM siRNA and lipofectamine 3000 (Thermo Fisher Scientific) according to manufacturer's instructions. All siRNAs used were purchased from Qiagen. The siRNA used as control (siCTRL) was Allstars negative control siRNA (Qiagen, Cat No./ID: 1027280). siRNAs targeting ACTN1 were siACTN1 #5 (Hs_ACTN1_5, SI00299131) and siACTN1 #2 (Hs_ACTN1_2, SI00021917). siRNAs targeting TNS3 were siTNS3 #1 (Hs_TENS1_1, SI00134372) and siTNS3 #2 (Hs_TNS3_2, SI02778643). siRNAs targeting TNS1 were siTNS1 #3 (Hs_TNS_3, SI00134106) and siTNS1 #4 (Hs_TNS_4, SI00134113). siRNAs targeting FERMT1 were siFERMT1 #5 (Hs_C20orf42_5, SI04269181), siFERMT1 #7 (Hs_C20orf42_7, SI04307219) and siFERMT1 #8 (Hs_C20orf42_8, SI04352978). siRNAs targeting FERMT2 were siFERMT2 #1 (Hs_FERMT2_1, SI04952542) and siFERMT2 #3 (Hs_FERMT2_3, SI04952556). siRNAs targeting CIB1 were siCIB1 #5 (Hs_CIB1_5, SI02657102) and siCIB #7 (Hs_CIB1_7, SI03164476). siRNAs targeting SHARPIN were siSHARPIN #2 (Hs_SHARPIN_2, SI00140182) and siSHARPIN #5 (Hs_SHARPIN_5, SI03067344). siRNA targeting ITGB1BP1 were si-ITGB1BP1 #5 (Hs_ITGB1BP1_5, SI03129385) and siITGB1BP1 #8 (Hs_ITGB1BP1_8, SI04332832). siRNA targeting TLN1 were siTLN1 #2 (Hs_TLN1_2, SI00086968)

and siTLN1 #3 (Hs_TLN1_3, SI00086975). siRNA targeting TLN2 was siTLN2 #3 (Hs_TLN2_3, SI00109277). siRNA targeting MYO10 were siMYO10 #5 (Hs_MYO10_5, SI04158245), siMYO10 #6 (Hs_MYO10_6, SI04252822) and siMYO10 #7 (Hs_MYO10_7, SI05085507).

SDS–PAGE and quantitative western blotting. Purified proteins or protein extracts were separated under denaturing conditions by SDS–PAGE and transferred to nitrocellulose membrane using Trans-Blot Turbo nitrocellulose transfer pack (Bio-Rad, 1704159). Membranes were blocked for 45 min at room temperature using 1x StartingBlock buffer (Thermo Fisher Scientific, 37578). After blocking membranes were incubated overnight with the appropriate primary antibody (1:1000 in PBS), washed three times in TBST and probed for 40 min using a fluorophore-conjugated secondary antibody diluted 1:5000 in the blocking buffer. Membranes were washed three times using TBST, over 15 min, and scanned using an Odyssey infrared imaging system (LI-COR Biosciences).

siRNA screen. 96-well glass-bottom plates (Cellvis, P96-1.5H-N) were first coated with a solution of poly-D-lysine (10 μg/ml in PBS, Sigma-Aldrich, A-003-M) at 4°C overnight. Plates were then washed with PBS and coated with a solution containing 10 μg/ml of bovine fibronectin (in PBS) also at 4°C overnight. Excess fibronectin was washed away with PBS. U2-OS cells stably expressing MYO10-GFP were silenced for the gene of interest using a panel of siRNAs (Qiagen flexiplate, 1704159) using Lipofectamine 3000 (Thermo Fisher Scientific, L3000075). 48 h post silencing, cells were trypsinized and plated on both fibronectin-coated 96-well glass-bottom plates and 96-well plastic-bottom plates in full culture medium. Cells plated in the plastic-bottom plates were allowed to spread for two hours before being lysed using an RNA extraction buffer. RNAs were then purified and the silencing efficiency of each siRNA was validated by qPCR analysis. Cells plated in the glass-bottom plates were allowed to spread for two hours and fixed with a warm solution of 4% paraformaldehyde (PFA, Thermo Scientific, 28906). After washing, the samples were incubated with a solution of 1 M Glycine (30 min, in PBS) and then for one hour in a solution containing phalloidin–Atto647N (1/400 in PBS, Thermo Fisher Scientific, 65906) and DAPI (0.5 μg/ml in PBS, Thermo Fisher Scientific, D1306). The 96-well glass-bottom plates were then imaged using a spinning-disk confocal microscope equipped with a 40x objective. Images were analysed using Fiji (Schindelin et al., 2012). Briefly, images were opened and, after background subtraction and normalization, MYO10 spots were automatically detected using Michael Schmid's 'Find maxima' plugin. As inactive MYO10 is known to accumulate in rab7 vesicles (Plantard et al., 2010), to obtain an accurate number of filopodia-specific MYO10 spots, intracellular MYO10 spots were excluded from the analysis. Intracellular MYO10 spots were automatically filtered by masking the cells using the F-actin staining. The remaining spots per field of view were counted.
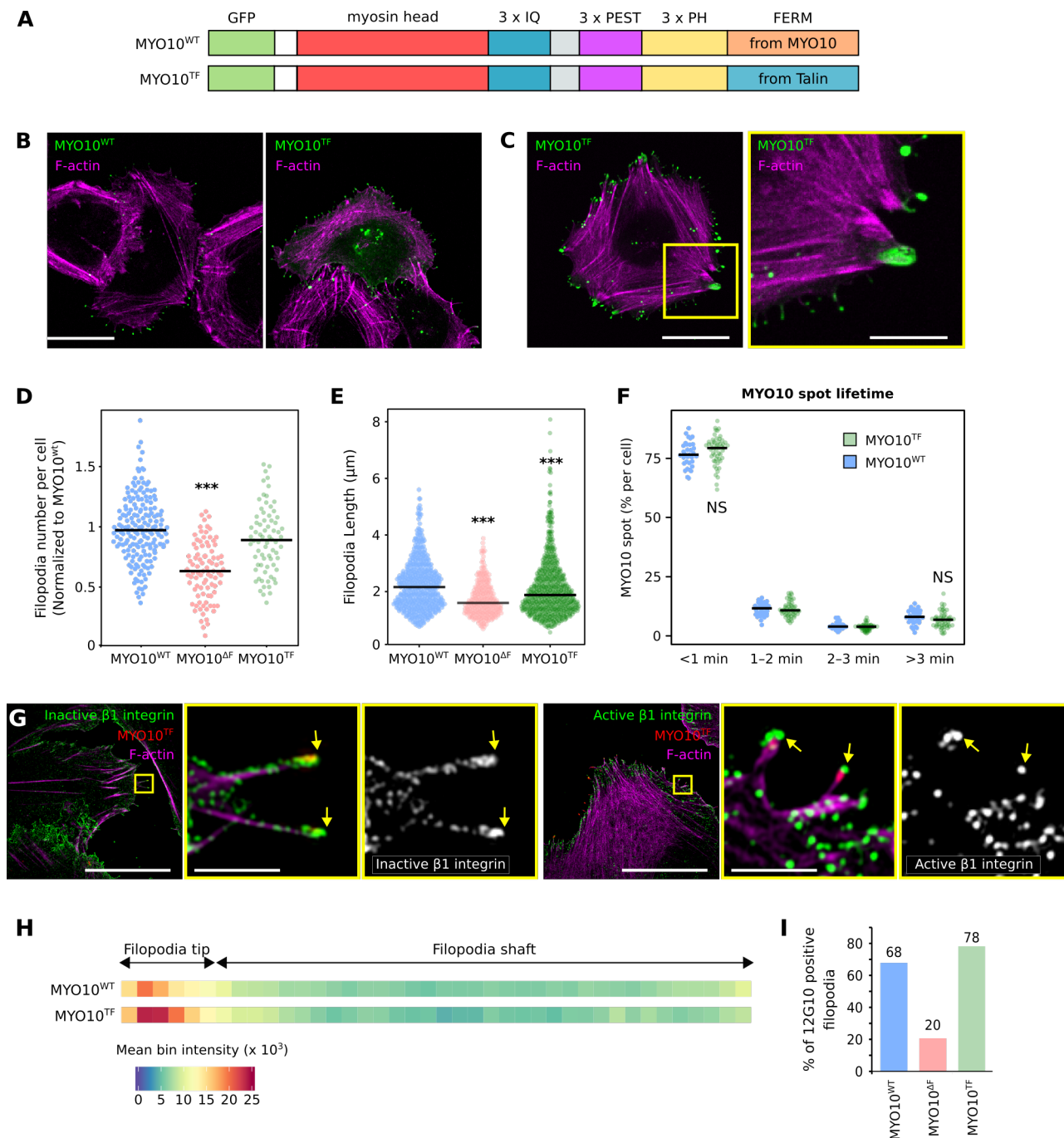
Fig. 5. MYO10-FERM domain fine-tunes integrin activity at filopodia tips. A) Cartoon illustrating the EGFP-MYO10^{WT} and EGFP-MYO10^{TF} constructs. **B-E**) U2-OS cells transiently expressing EGFP-MYO10^{WT} or EGFP-MYO10^{TF} were plated on fibronectin for 2 h, fixed and imaged using a spinning-disk confocal microscope or an Airyscan confocal microscope. **B**) Representative MIPs acquired on a spinning-disk confocal are displayed. Scale bar: 25 μm. **C**) An image acquired on an Airyscan confocal microscope is displayed. The yellow square highlights an ROI, which is magnified. scale bars: (main) 25 μm; (inset) 5 μm. **D**) The number of MYO10-positive filopodia per cell was quantified (EGP-MYO10^{WT}, n = 33 cells; EGFP-MYO10^{ΔF}, n = 53 cells; EGFP-MYO10^{TF}, n = 53 cells; three biological repeats; *** p-value < 0.001, * p-value = 0.043). **E**) Quantification of filopodia length in U2-OS cells transiently expressing EGFP-MYO10^{WT}, EGFP-MYO10^{ΔF} or EGFP-MYO10^{TF} quantified from SIM images. Results of EGFP-MYO10^{ΔF} were already displayed in figure 2 and are provided here again as reference (EGFP-MYO10^{WT}, n = 512 filopodia; EGFP-MYO10^{ΔF}, n = 283 filopodia; EGFP-MYO10^{TF} n = 669 filopodia ; three biological repeats; *** p-value = <0.001). **F**) U2-OS cells expressing EGFP-MYO10^{WT} or EGFP-MYO10^{TF} were plated on fibronectin and imaged live using an Airyscan confocal microscope (1 picture every 5 s over 20 min). For each condition, MYO10-positive particles were automatically tracked, and MYO10 spot lifetime (calculated as a percentage of the total number of filopodia generated per cell) was plotted and displayed as boxplots (three biological repeats, EGP-MYO10^{WT}, n= 33 cells; EGFP-MYO10^{TF}, n= 53 cells). **G**) U2-OS cells expressing EGFP-MYO10^{TF} were plated on fibronectin 2 h, stained for active (clone 12G10) or inactive (clone 4B4) β1 integrin and F-actin, and imaged using SIM. Representative MIPs are displayed. The yellow squares highlight ROIs, which are magnified; yellow arrows highlight filopodia tips; scale bars: (main) 20 μm; (inset) 2 μm. **H**) Heatmap highlighting the sub-filopodial localisation of active β1 integrin in cells expressing EGFP-MYO10^{WT} or EGFP-MYO10^{TF} (EGFP-MYO10^{WT}, n = 512 filopodia; EGFP-MYO10^{TF}, n = 669 filopodia; three biological repeats). **I**) Bar chart highlighting the percentage of filopodia with detectable levels of active β1 integrin in U2-OS cells expressing EGFP-MYO10^{WT}, EGFP-MYO10^{ΔF} or EGFP-MYO10^{TF} (EGFP-MYO10^{WT}, n = 512 filopodia; EGFP-MYO10^{ΔF}, n = 283 filopodia; EGFP-MYO10^{TF} n = 669 filopodia; three biological repeats). For all panels, p-values were determined using a randomization test. NS indicates no statistical difference between the mean values of the highlighted condition and the control.

RNA extraction, cDNA preparation and Taq-Man qPCR. Total RNA extracted using the NucleoSpin RNA Kit (Macherey-Nagel, 740955.240C) was reverse transcribed into cDNA using the high-capacity cDNA reverse transcription kit (Applied Biosystems, Thermo Fisher Scientific, 43-688-14) according to the manufacturer's instructions. The TaqMan primer sequences and associated universal probes were generated using ProbeFinder (version 2.53, Roche). The primers themselves were ordered from IDT, and the Taq-Man fast advanced master mix (Thermo Fisher Scientific, 4444557) was used to perform the qPCR reactions according to the manufacturer's instructions. Primers used in this study were against TNS1 (cca gac acc cac ctg act tag; ttg gtg cat tct cag tgg tg; probe 58), ACTN1 (gcc tca tca gct tgg gtt at; cat gat gcg ggc aaa ttc; probe 7), FERMT1 (aga cgt cac act gag agt atc tgg; tct gac cag tct tgg gat ata ttg; probe 25), TNS3 (agg ctg cct gac aca gga; ;agg ggc tgt tca gca gag; probe 57), TLN1 (ccc tta cct ggg gag aca at; gag ctc acg gct ttg gtg; probe 61), CIB1 (agt tcc agc acg tca tct cc; gct gct gtc aca gga caa tc; probe 17), ITGB1BP (ttg aag ggc cat tag acc tg; gaa caa aag gca act ttc cat c; probe 61), FERMT2 (taa aa cat ggc gtt tca gca; cat ctg caa act cta cgg tgac; probe 48), SHARPIN (ccc tgg ctg tga gat gtg ta; ggc cac tct ccc ctt gta ac; probe 83), FLNA (gtc acc ggt cgc tct cag; agg gga cgg ccc ttt aat; probe 32) and TLN2 (ggt cat ggt tgg gca gat; gca tgc ttg tgt tga tgg tc; probe 40). qPCR reactions were analysed with the 7900HT fast RT-PCR System (Applied Biosystems), and the results were analysed using the RQ Manager Software (Applied Biosystems). Relative expression was calculated by the $2^{-\Delta\Delta CT}$ method. GAPDH mRNA levels were used to normalise data between experiments and conditions.

Generation of the filopodia maps. U2-OS cells transiently expressing the constructs of interests were plated on high tolerance glass-bottom dishes (MatTek Corporation, coverslip #1.7) pre-coated first with Poly-L-lysine (10 μg/ml, 1 h at 37°C) and then with bovine plasma fibronectin (10 μg/ml, 2 h at 37°C). After 2 h, samples were fixed and permeabilised simultaneously using a solution of 4% PFA and 0.25% (vol/vol) Triton X-100 for 10 min. Cells were then washed with PBS, quenched using a solution of 1 M glycine for 30 min, and, when appropriate, incubated with the primary antibody for 1 h (1:100). After three washes, cells were incubated with a secondary antibody for 1 h (1:100). Samples were then washed three times and incubated with SiR-actin (100 nM in PBS; Cytoskeleton; catalogue number: CY-SC001) at 4°C until imaging (minimum length of staining, overnight at 4°C; maximum length, one week). Just before imaging, samples were washed three times in PBS and mounted in vectashield (Vector Laboratories).

To map the localisation of each protein within filopodia, images were first processed in Fiji (Schindelin et al., 2012) and data analysed using R as previously described (Jacquemet et al., 2019). Briefly, in Fiji, the brightness and contrast of each image was automatically adjusted using, as an upper maximum, the brightest cellular structure labelled in the field of view. In Fiji, line intensity profiles (1-pixel width) were manually drawn from filopodium tip to base (defined by the intersection of the filopodium and the lamellipodium). To avoid any bias in the analysis, the intensity profile lines were drawn from a merged image. All visible filopodia in each image were analysed and exported for further analysis (export was performed using the "Multi Plot" function). For each staining, line intensity profiles were then compiled and analysed in R. To homogenise filopodia length; each line intensity profile was binned into 40 bins (using the median value of pixels in each bin and the R function "tapply"). Using the line intensity profiles, the percentage of filopodia positive for active β1 at their tip was quantified. A positive identification was defined as requiring at least an average value of 5000 (values between 0-65535) within the bins defining the filopodium tip (identified using MYO10 staining). The map of each protein of interest was created by averaging hundreds of binned intensity profiles. The length of each filopodia analysed were directly extracted from the line intensity profiles.

Quantification of filopodia numbers and dynamics. For the filopodia formation assays, cells were plated on fibronectin-coated glass-bottom dishes (MatTek Corporation) for 2 h. Samples were fixed for 10 min using a solution of 4% (wt/vol) PFA, then permeabilized using a solution of 0.25% (vol/vol) Triton X-100 for 3 min. Cells were then washed with PBS and quenched using a solution of 1 M glycine for 30 min. Samples were then washed three times in PBS and stored in PBS containing SiR-actin (100 nM; Cytoskeleton; catalogue number: CY-SC001) at 4°C until imaging. Just before imaging, samples were washed three times in PBS. Images were acquired using a spinning-disk confocal microscope (100x objective). The number of filopodia per cell was manually scored using Fiji (Schindelin et al., 2012). To study filopodia stability, U2-OS cells expressing MYO10-GFP were plated for at least 2 h on fibronectin before the start of live imaging (pictures taken every 5 s at 37°C, on an Airyscan microscope, using a 40x objective). All live-cell imaging experiments were performed in normal growth media, supplemented with 50 mM HEPES, at 37°C and in the presence of 5% CO_2. Filopodia lifetimes were then measured by identifying and tracking all MYO10 spots using the Fiji plugin TrackMate (Tinevez et al., 2017). In TrackMate, the LoG detector (estimated bob diameter = 0.8 mm; threshold = 20; subpixel localization enabled) and the simple LAP tracker (linking max distance = 1 mm; gap-closing max distance = 1 mm; gap-closing max frame gap = 0) were used.

Light microscopy setup. The spinning-disk confocal microscope (spinning-disk confocal) used was a Marianas spinning-disk imaging system with a Yokogawa CSU-W1 scanning unit on an inverted Zeiss Axio Observer Z1 microscope controlled by SlideBook 6 (Intelligent Imaging Innovations, Inc.). Images were acquired using either an Orca Flash 4 sCMOS camera (chip size 2048 × 2048; Hamamatsu Photonics) or an Evolve 512 EMCCD camera (chip size 512 × 512; Photometrics). Objectives used were a 40x water (NA 1.1, LD C-Apochromat, Zeiss), a 63× oil (NA 1.4, Plan-Apochromat, M27 with DIC III Prism, Zeiss) and a

100x oil (NA 1.4 oil, Plan-Apochromat, M27) objective. The structured illumination microscope (SIM) used was DeltaVision OMX v4 (GE Healthcare Life Sciences) fitted with a 60x Plan-Apochromat objective lens, 1.42 NA (immersion oil RI of 1.516) used in SIM illumination mode (five phases x three rotations). Emitted light was collected on a front-illuminated pco.edge sCMOS (pixel size 6.5 mm, readout speed 95 MHz; PCO AG) controlled by SoftWorx. The confocal microscope used was a laser scanning confocal microscope LSM880 (Zeiss) equipped with an Airyscan detector (Carl Zeiss) and a 40x oil (NA 1.4) objective. The microscope was controlled using Zen Black (2.3), and the Airyscan was used in standard super-resolution mode.

Integrin activity assays. CHO cells detached using Hyclone HyQTase (Thermo Fisher Scientific, SV300.30.01) were pretreated for 10 min with 5 mM EDTA, or with PBS and then incubated for 40 min with Alexa Fluor 647 labelled fibronectin fragment (FN 7-10). After washing away the unbound fibronectin (using Tyrode's buffer: 10 mM HEPES-NaOH, pH 7.5, 137 mM NaCl, 2.68 mM KCl, 0.42 mM NaH_2PO_4, 1.7 mM $MgCl_2$, 11.9 mM $NaHCO_3$, 5 mM glucose, and 0.1% BSA), cells were fixed with 4% of PFA (in PBS) for 10 min at room temperature. Part of the HyQTase treated cells were also fixed with 4% PFA (in PBS) and stained with an anti-α5 integrin antibody (2 h at 4°C, 1:10 in PBS, clone PB1, Developmental studies hybridoma bank) and with an Alexa Fluor 647-conjugated secondary antibody (45 min at RT, 1:200 in PBS, Thermo Fisher Scientific, A-21235). Fluorescence intensity was recorded using FACS (BD LSRFortessa™). Data were gated and analyzed using the Flowing Software. The integrin activity index (AI) was calculated as indicated bellow, where F = FN7-10 signal, F_{EDTA} = FN7-10 signal in EDTA treated cells and F_{PB1} = α5 integrin signal.

$$AI = \frac{(F - F_{EDTA})}{F_{PB1}} \quad \textbf{(1)}$$

MDA-MB-231 and U2-OS cells detached using Hyclone HyQTase (Thermo Fisher Scientific, SV300.30.01) were fixed with 4% PFA (in PBS) for 10 min and stained for active (clone 9EG7) and total β1 integrin (clone P5D2) overnight at 4°C. Cells were then stained with the appropriate Alexa Fluor 647-conjugated secondary antibody (45 min at RT, 1:200, Thermo Fisher Scientific) and the fluorescence was recorded using FACS. Data were gated and analyzed using the Flowing Software, and the integrin activity (IA) was calculated as indicated below where F_{9EG7} and F_{P5D2} are the signals intensities of the 9EG7 and P5D2 stainings, respectively. $F_{2nd\,Ab}$ corresponds to the signal intensity recorded when the cells are stained with only the secondary antibody.

$$IA = \frac{F_{9EG7} - F_{2ndAb}}{F_{P5D2} - F_{2ndAb}} \quad \textbf{(2)}$$

FACS FRET. FACS data acquisition was performed with LSRFortessa™ flow cytometer (BD Biosciences) controlled by the BD FACSDiva™ software. To excite and detect mTurquoise2 and YPet fluorophores, a 504 nm laser line together with a filter set composed of a 475 long-pass filter and a narrow 540/30 nm filter was used. To detect the mCherry fluorophore, a 561 nm laser line was used together with a filter set composed of a 600 nm long-pass filter and a narrow 610/20 nm filter. FRET was estimated in mTurquoise2/YPet/mCherry triple-positive cells by measuring the fluorescent signal intensity recorded in the 540/30 nm channel (FRET channel) following 504 nm excitation. The FRET channel intensity (Fig 4H and 4I) was calculated, for each condition, as the average of the signal intensity measured in the FRET channel (10 000 cells per condition) normalised to the sum of the mean of each condition. Results are plotted as bar charts where each biological repeat is displayed as a data point. Raw data were analysed using the Flowing Software v. 2.5. FPbase spectra viewer was used to aid in the selection of the laser-lines and filter sets before starting the experiments (Lambert, 2019).

Cell spreading assay. The xCELLigence RTCA instrument (Roche) was used to measure cell adhesion on fibronectin in real-time (Hamidi et al., 2017). The RTCA instrument uses gold-bottom electrode plates to measure the impedance between two electrodes. This is expressed as an arbitrary cell index value. The xCELLigence 96-well plates (Acea Biosciences, E-Plate VIEW 96 PET, 00300600900) were coated with a solution of 20 μg/ml of poly-D-lysine (in PBS) for 1 h at 37°C, washed with PBS, and coated with a solution of 10 μg/ml fibronectin (in PBS) for 1 h at 37°C. Plates were then blocked using a solution of 1% BSA (in PBS) for 1 h in RT. After 2 PBS washes, 15000 cells were seeded into each well in serum-free culture medium. The cell index was recorded over time.

Recombinant protein expression and purification. The E. coli BL-21(DE3) strain was transformed with IPTG inducible, His-tagged expression constructs, and the transformed bacteria were grown at 37°C in LB media supplemented with ampicillin (1 mg/ml) until OD600 was 0.6-0.8. Protein expression was then induced using IPTG (0.5 mM), and the temperature was lowered to 25°C. Cells were harvested after 5 h by centrifugation (20 min at 6000 g). Bacteria were then resuspended in a resuspension buffer (1x TBS, cOmplete™ protease inhibitor tablet (Roche, cat. no. 5056489001), 1x AEBSF inhibitor, 1x PMSF, RNase 0.05 mg/ml, DNase 0.05 mg/ml). To lyse the bacteria, a small spoonful of lysozyme and 1x BugBuster (Merck Millipore, cat. no. 70584-4) were added, and the suspension was agitated for 30 min at 4°C. Cell debris was pelleted using a JA25.5 rotor at 20000 rpm for 1 h. His-tagged proteins were batch purified from the supernatant using a Protino Ni-TED 2000 column (Macherey Nagel, cat. no. 745120.25) according to manufacturer's instructions. Proteins were eluted using the elution buffer provided with the kit supplemented with 1 mM AEBSF. For each purified protein, several 1 ml fractions were collected, ran on a 4-20% protein gel (Bio-Rad Mini-PROTEAN TGX, #4561093), stained with Instant-Blue® (Expedeon, ISB1L) and the fractions abundant in

tagged protein were combined. Imidazole was removed in a buffer exchange overnight at 4°C and 1 mM AEBSF was added to the imidazole-free protein. Proteins were stored at 4°C for up to one week.

Whole-mount immuno-SEM. U2-OS cells expressing MYO10-GFP were plated for 2 h on fibronectin-coated coverslips and fixed with a solution of 4% PFA (in 0.1 M HEPES, pH 7.3) for 30 min. After washing and quenching with 50 mM NH4Cl (in 0.1 M HEPES), non-specific binding was blocked with a buffer containing 2% BSA (in 0.1 M HEPES). Samples were then labelled using the appropriate primary antibody (1:10 in 0.1 M HEPES) for 30 min, washed, and labelled with a gold conjugated secondary antibody (1:50 in 0.1 M HEPES, 30 nm gold particles, BBI solutions, EM.GAF30) for 30 min. After immunolabeling, the samples were washed, and post-fixed with a solution of 2.5% glutaraldehyde and 1% buffered osmium tetroxide prior to dehydration and drying using hexamethyldisilazane. The dried samples were mounted on SEM stubs and sputter-coated with carbon. The micrographs were acquired with FEI Quanta FEG 250 microscope with SE and vC detectors (FEI Comp.) using an acceleration voltage of 5.00 kV and a working distance ranging from 7.7 to 10.9 mm.

Integrin tail pull-downs. For each pulldown, 20 µl of streptavidin Dynabeads (MyOne Streptavidin C1, Invitrogen, 65001) were incubated, for 30 min, on ice, with the appropriate biotinylated integrin tail peptides (LifeTein). U2-OS cells were washed twice with cold PBS and lysed on ice with a buffer containing 40 mM HEPES, 75 mM NaCl, 2 mM EDTA, 1% NP-40, a cOmplete™ protease inhibitor tablet (Roche, 5056489001) and a phosphatase-inhibitor tablet (Roche, 04906837001). Samples were cleared by centrifugation (13,000 g, 10 min) and incubated with the streptavidin Dynabeads for 2 h at 4°C. Beads were washed three times with a washing buffer (50 mM Tris-HCl pH 7.5, 150 mM NaCl, 1% (v/v) NP-40) and proteins bound to the beads were eluted using SDS sample buffer and heated 5-10 min at 90°C. Results were analyzed using western blot. Integrin peptides used were wild-type β1-integrin tail (KLLMIIHDRREFAK-FEKEKMNAKWDTGENPIYKSAVTTVVNPKYEGK), the β1-integrin tail where the NPXY motif is deleted (KLLMI-IHDRREFAKFEKEKMNAKWDTGEN), the conserved region of the α2-integrin tail (WKLGFFKRKYEKM), the conserved region of α2-integrin tail peptide where the GFFKR motif is mutated (GAAKR mutant, WKLGAAKRKYEKM) and the wild-type α5-integrin tail (KLGFFKRSLPYG-TAMEKAQLKPPATSDA).

Microscale thermophoresis. Recombinant His-tagged proteins were labelled using the Monolith His-Tag Labeling Kit RED-tris-NTA (NanoTemper, MO-L008). In all experiments, the labelled His-tagged recombinant proteins were used at a concentration of 20 nM while the integrin tail peptides were used at increasing concentration. Kd values were calculated using the equation provided below (Eq.1), where Kd is the dissociation constant, [A] the concentration of the

free fluorescent molecule, [L] the concentration of the free ligand, [AL] the concentration of the AL-complex. [A0] is the known concentration of the fluorescent molecule and [L0] is the known concentration of added ligand. This leads to a quadratic fitting function for [AL]:

$$[AL] = \left(\tfrac{1}{2}\right) \times \left(([A0]+[L0]+Kd) - (([A0]+[L0]+Kd)^2 - 4\times[A0]\times[L0])^{\tfrac{1}{2}} \right)$$
$$(3)$$

Alternatively, binding was also expressed as a change in MST signal (normalized fluorescence ΔFnorm). This is defined as a ratio:

$$\Delta Fnorm = F1/F0 \qquad (4)$$

Where F0 is the fluorescence prior and F1 after IR laser activation.

All binding data were analyzed using MO.Control and MO.Affinity software (NanoTemper).

Quantification and statistical analysis. Randomization tests were performed using the online tool PlotsOfDifferences (Goedhart, 2019). Dot plots were generated using PlotsOfData (Postma and Goedhart, 2019). Bar plots with visualized data points, time-series data and density plots were generated using R, Rstudio (Integrated Development for R. RStudio, Inc., Boston, MA) and ggplot2 (Wickham, 2016). Other statistical analyses were performed using Google sheets except for the one-sample t-test which was performed using an online calculator.

Data availability. The authors declare that the data supporting the findings of this study are available within the article and from the authors on request.

Conflict of interest. The authors declare no competing interests.

CellMech) and by Drug Discovery and Diagnostics strategic funding to Åbo Akademi University (G.J.). M.M. has been supported by the Drug Research Doctoral Programme, University of Turku foundation, Maud Kuistila foundation, Instrumentarium Foundation, Lounais Suomen syöpäyhdistys, K. Albin Johansson's foundation and Ida Montini foundation. B.G. was supported by the Biotechnology and Biological Sciences Research Council grant BB/N007336/1.

EXTENDED AUTHOR INFORMATION

- Mitro Miihkinen: 0000-0001-6822-3647; mitroe
- Max L.B. Grönloh: GronlohMax
- Helena Vihinen: 0000-0003-3862-9237;
- Eija Jokitalo: 0000-0002-4159-6934; EJokitalo
- Benjamin T. Goult: 0000-0002-3438-2807; bengoult
- Johanna Ivaska: 0000-0002-6295-6556; johannaivaska
- Guillaume Jacquemet: 0000-0002-9286-920X; guijacquemet

Bibliography

Alanko, J., A. Mai, G. Jacquemet, K. Schauer, R. Kaukonen, M. Saari, B. Goud, and J. Ivaska. 2015. Integrin endosomal signalling suppresses anoikis. Nat. Cell Biol. 17:1412–1421.

Alieva, N.O., A.K. Efremov, S. Hu, D. Oh, Z. Chen, M. Natarajan, H.T. Ong, A. Jégou, G. Romet-Lemonne, J.T. Groves, M.P. Sheetz, J. Yan, and A.D. Bershadsky. 2019. Myosin IIA and formin dependent mechanosensitivity of filopodia adhesion. Nat. Commun. 10:1–14. doi:10.1038/s41467-019-10964-w.

Anthis, N.J., K.L. Wegener, F. Ye, C. Kim, B.T. Goult, E.D. Lowe, I. Vakonakis, N. Bate, D.R. Critchley, M.H. Ginsberg, and I.D. Campbell. 2009. The structure of an integrin/talin complex reveals the basis of inside-out signal transduction. EMBO J. 28:3623–3632. doi:10.1038/emboj.2009.287.

Arjonen, A., R. Kaukonen, E. Mattila, P. Rouhi, G. Högnäs, H. Sihto, B.W. Miller, J.P. Morton, E. Bucher, P. Taimen, R. Virtakoivu, Y. Cao, O.J. Sansom, H. Joensuu, and J. Ivaska. 2014. Mutant p53-associated myosin-X upregulation promotes breast cancer invasion and metastasis. J. Clin. Invest. 124:1069–1082. doi:10.1172/JCI67280.

Askari, J.A., P.A. Buckley, A.P. Mould, and M.J. Humphries. 2009. Linking integrin conformation to function. J. Cell Sci. 122:165–170. doi:10.1242/jcs.018556.

Bennett, R.D., A.S. Mauer, and E.E. Strehler. 2007. Calmodulin-like protein increases filopodia-dependent cell motility via up-regulation of myosin-10. J. Biol. Chem. 282:3205–3212. doi:10.1074/jbc.M607174200.

Berg, J.S., and R.E. Cheney. 2002. Myosin-X is an unconventional myosin that undergoes intrafilopodial motility. Nat. Cell Biol. 4:246–250. doi:10.1038/ncb762.

Bindels, D.S., L. Haarbosch, L. van Weeren, M. Postma, K.E. Wiese, M. Mastop, S. Aumonier, G. Gotthard, A. Royant, M.A. Hink, and T.W.J.G. Jr. 2017. mScarlet: a bright monomeric red fluorescent protein for cellular imaging. Nat. Methods. 14:53–56. doi:10.1038/nmeth.4074.

Bornschlögl, T., S. Romero, C.L. Vestergaard, J.-F. Joanny, G.T.V. Nhieu, and P. Bassereau. 2013. Filopodial retraction force is generated by cortical actin dynamics and controlled by reversible tethering at the tip. Proc. Natl. Acad. Sci. 110:18928–18933. doi:10.1073/pnas.1316572110.

Braniš, J., C. Pataki, M. Spörrer, R.C. Gerum, A. Mainka, V. Cermak, W.H. Goldmann, B. Fabry, J. Brabek, and D. Rosel. 2017. The role of focal adhesion anchoring domains of CAS in mechanotransduction. Sci. Rep. 7:1–12. doi:10.1038/srep46233.

Byron, A., J.D. Humphries, J.A. Askari, S.E. Craig, A.P. Mould, and M.J. Humphries. 2009. Anti-integrin monoclonal antibodies. J. Cell Sci. 122:4009–4011. doi:10.1242/jcs.056770.

Chinthalapudi, K., E.S. Rangarajan, and T. Izard. 2018. The interaction of talin with the cell membrane is essential for integrin activation and focal adhesion formation. Proc. Natl. Acad. Sci. 115:10339–10344. doi:10.1073/pnas.1806275115.

Conway, J.R.W., and G. Jacquemet. 2019. Cell matrix adhesion in cell migration. Essays Biochem. 63:535–551. doi:10.1042/EBC20190012.

De Franceschi, N., A. Arjonen, N. Elkhatib, K. Denessiouk, A.G. Wrobel, T.A. Wilson, J. Pouwels, G. Montagnac, D.J. Owen, and J. Ivaska. 2016. Selective integrin endocytosis is driven by interactions between the integrin α-chain and AP2. Nat. Struct. Mol. Biol. 23:172–179. doi:10.1038/nsmb.3161.

Elliott, P.R., B.T. Goult, P.M. Kopp, N. Bate, J.G. Grossmann, G.C.K. Roberts, D.R. Critchley, and I.L. Barsukov. 2010. The Structure of the Talin Head Reveals a Novel Extended Conformation of the FERM Domain. Structure. 18:1289–1299. doi:10.1016/j.str.2010.07.011.

Franceschi, N.D., M. Miihkinen, H. Hamidi, J. Alanko, A. Mai, L. Picas, C. Guzmán, D. Lévy, P. Mattjus, B.T. Goult, B. Goud, and J. Ivaska. 2019. ProLIF – quantitative integrin protein–protein interactions and synergistic membrane effects on proteoliposomes. J. Cell Sci. 132. doi:10.1242/jcs.214270.

Gallop, J.L. 2019. Filopodia and their links with membrane traffic and cell adhesion. Semin. Cell Dev. Biol. doi:10.1016/j.semcdb.2019.11.017.

Gingras, A.R., F. Lagarrigue, M.N. Cuevas, A.J. Valadez, M. Zorovich, W. McLaughlin, M.A. Lopez-Ramirez, N. Seban, K. Ley, W.B. Kiosses, and M.H. Ginsberg. 2019. Rap1 binding and a lipid-dependent helix in talin F1 domain promote integrin activation in tandem. J. Cell Biol. 218:1799–1809. doi:10.1083/jcb.201810061.

Goedhart, J. 2019. PlotsOfDifferences – a web app for the quantitative comparison of unpaired data. bioRxiv. 578575. doi:10.1101/578575.

Goult, B.T., N. Bate, N.J. Anthis, K.L. Wegener, A.R. Gingras, B. Patel, I.L. Barsukov, I.D. Campbell, G.C.K. Roberts, and D.R. Critchley. 2009. The Structure of an Interdomain Complex That Regulates Talin Activity. J. Biol.

Chem. 284:15097–15106. doi:10.1074/jbc.M900078200.

Goult, B.T., M. Bouaouina, P.R. Elliott, N. Bate, B. Patel, A.R. Gingras, J.G. Grossmann, G.C.K. Roberts, D.A. Calderwood, D.R. Critchley, and I.L. Barsukov. 2010. Structure of a double ubiquitin-like domain in the talin head: a role in integrin activation. EMBO J. 29:1069–1080. doi:10.1038/emboj.2010.4.

Hamidi, H., J. Lilja, and J. Ivaska. 2017. Using xCELLigence RTCA Instrument to Measure Cell Adhesion. BioProtoc. 7. doi:10.21769/BioProtoc.2646.

He, K., T. Sakai, Y. Tsukasaki, T.M. Watanabe, and M. Ikebe. 2017. Myosin X is recruited to nascent focal adhesions at the leading edge and induces multi-cycle filopodial elongation. Sci. Rep. 7:1–12. doi:10.1038/s41598-017-06147-6.

Hirano, Y., T. Hatano, A. Takahashi, M. Toriyama, N. Inagaki, and T. Hakoshima. 2011. Structural basis of cargo recognition by the myosin-X MyTH4-FERM domain. EMBO J. 30:2734–2747. doi:10.1038/emboj.2011.177.

Hu, W., B. Wehrle-Haller, and V. Vogel. 2014. Maturation of filopodia shaft adhesions is upregulated by local cycles of lamellipodia advancements and retractions. PloS One. 9:e107097. doi:10.1371/journal.pone.0107097.

Jacquemet, G., H. Baghirov, M. Georgiadou, H. Sihto, E. Peuhu, P. Cettour-Janet, T. He, M. Perälä, P. Kronqvist, H. Joensuu, and J. Ivaska. 2016. L-type calcium channels regulate filopodia stability and cancer cell invasion downstream of integrin signalling. Nat. Commun. 7:13297. doi:10.1038/ncomms13297.

Jacquemet, G., D.M. Green, R.E. Bridgewater, A. von Kriegsheim, M.J. Humphries, J.C. Norman, and P.T. Caswell. 2013. RCP-driven α5β1 recycling suppresses Rac and promotes RhoA activity via the RacGAP1-IQGAP1 complex. J. Cell Biol. 202:917–935. doi:10.1083/jcb.201302041.

Jacquemet, G., H. Hamidi, and J. Ivaska. 2015. Filopodia in cell adhesion, 3D migration and cancer cell invasion. Curr. Opin. Cell Biol. 36:23–31. doi:10.1016/j.ceb.2015.06.007.

Jacquemet, G., I. Paatero, A.F. Carisey, A. Padzik, J.S. Orange, H. Hamidi, and J. Ivaska. 2017. FiloQuant reveals increased filopodia density during breast cancer progression. J. Cell Biol. 216:3387–3403. doi:10.1083/jcb.201704045.

Jacquemet, G., A. Stubb, R. Saup, M. Miihkinen, E. Kremneva, H. Hamidi, and J. Ivaska. 2019. Filopodome Mapping Identifies p130Cas as a Mechanosensitive Regulator of Filopodia Stability. Curr. Biol. CB. 29:202-216.e7. doi:10.1016/j.cub.2018.11.053.

Jerabek-Willemsen, M., T. André, R. Wanner, H.M. Roth, S. Duhr, P. Baaske, and D. Breitsprecher. 2014. MicroScale Thermophoresis: Interaction analysis and beyond. J. Mol. Struct. 1077:101–113. doi:10.1016/j.molstruc.2014.03.009.

Jones, M.C., J.A. Askari, J.D. Humphries, and M.J. Humphries. 2018. Cell adhesion is regulated by CDK1 during the cell cycle. J. Cell Biol. 217:3203–3218. doi:10.1083/jcb.201802088.

Kopp, P.M., N. Bate, T.M. Hansen, N.P.J. Brindle, U.

Praekelt, E. Debrand, S. Coleman, D. Mazzeo, B.T. Goult, A.R. Gingras, C.A. Pritchard, D.R. Critchley, and S.J. Monkley. 2010. Studies on the morphology and spreading of human endothelial cells define key inter- and intramolecular interactions for talin1. Eur. J. Cell Biol. 89:661–673. doi:10.1016/j.ejcb.2010.05.003.

Lagarrigue, F., P. Vikas Anekal, H.-S. Lee, A.I. Bachir, J.N. Ablack, A.F. Horwitz, and M.H. Ginsberg. 2015. A RIAM/lamellipodin-talin-integrin complex forms the tip of sticky fingers that guide cell migration. Nat. Commun. 6:8492. doi:10.1038/ncomms9492.

Lambert, T.J. 2019. FPbase: a community-editable fluorescent protein database. Nat. Methods. 16:277–278. doi:10.1038/s41592-019-0352-8.

Lilja, J., T. Zacharchenko, M. Georgiadou, G. Jacquemet, N. De Franceschi, E. Peuhu, H. Hamidi, J. Pouwels, V. Martens, F.H. Nia, M. Beifuss, T. Boeckers, H.-J. Kreienkamp, I.L. Barsukov, and J. Ivaska. 2017. SHANK proteins limit integrin activation by directly interacting with Rap1 and R-Ras. Nat. Cell Biol. 19:292–305. doi:10.1038/ncb3487.

Lin, W.-H., J.T. Hurley, A.N. Raines, R.E. Cheney, and D.J. Webb. 2013. Myosin X and its motorless isoform differentially modulate dendritic spine development by regulating trafficking and retention of vasodilator-stimulated phosphoprotein. J. Cell Sci. 126:4756–4768. doi:10.1242/jcs.132969.

Liu, J., M. Das, J. Yang, S.S. Ithychanda, V.P. Yakubenko, E.F. Plow, and J. Qin. 2015. Structural mechanism of integrin inactivation by filamin. Nat. Struct. Mol. Biol. 22:383–389. doi:10.1038/nsmb.2999.

Mattila, P.K., and P. Lappalainen. 2008. Filopodia: molecular architecture and cellular functions. Nat. Rev. Mol. Cell Biol. 9:446–454. doi:10.1038/nrm2406.

Paul, N.R., J.L. Allen, A. Chapman, M. Morlan-Mairal, E. Zindy, G. Jacquemet, L. Fernandez del Ama, N. Ferizovic, D.M. Green, J.D. Howe, E. Ehler, A. Hurlstone, and P.T. Caswell. 2015. α5β1 integrin recycling promotes Arp2/3-independent cancer cell invasion via the formin FHOD3. J. Cell Biol. 210:1013–1031. doi:10.1083/jcb.201502040.

Pellinen, T., A. Arjonen, K. Vuoriluoto, K. Kallio, J.A.M. Fransen, and J. Ivaska. 2006. Small GTPase Rab21 regulates cell adhesion and controls endosomal traffic of β1-integrins. J. Cell Biol. 173:767–780. doi:10.1083/jcb.200509019.

Plantard, L., A. Arjonen, J.G. Lock, G. Nurani, J. Ivaska, and S. Strömblad. 2010. PtdIns(3,4,5)P is a regulator of myosin-X localization and filopodia formation. J. Cell Sci. 123:3525–3534. doi:10.1242/jcs.069609.

Postma, M., and J. Goedhart. 2019. PlotsOfData—A web app for visualizing data together with their summaries. PLOS Biol. 17:e3000202. doi:10.1371/journal.pbio.3000202.

Robertson, J., G. Jacquemet, A. Byron, M.C. Jones, S. Warwood, J.N. Selley, D. Knight, J.D. Humphries, and M.J. Humphries. 2015. Defining the phospho-adhesome through the phosphoproteomic analysis of integrin signalling. Nat.

Commun. 6:6265. doi:10.1038/ncomms7265.

Schindelin, J., I. Arganda-Carreras, E. Frise, V. Kaynig, M. Longair, T. Pietzsch, S. Preibisch, C. Rueden, S. Saalfeld, B. Schmid, J.-Y. Tinevez, D.J. White, V. Hartenstein, K. Eliceiri, P. Tomancak, and A. Cardona. 2012. Fiji: an open-source platform for biological-image analysis. Nat. Methods. 9:676–682. doi:10.1038/nmeth.2019.

Shibue, T., M.W. Brooks, M.F. Inan, F. Reinhardt, and R.A. Weinberg. 2012. The outgrowth of micrometastases is enabled by the formation of filopodium-like protrusions. Cancer Discov. 2:706–721. doi:10.1158/2159-8290.CD-11-0239.

Stubb, A., R.F. Laine, M. Miihkinen, H. Hamidi, C. Guzmán, R. Henriques, G. Jacquemet, and J. Ivaska. 2020. Fluctuation-Based Super-Resolution Traction Force Microscopy. Nano Lett. 20:2230–2245. doi:10.1021/acs.nanolett.9b04083.

Sun, Z., M. Costell, and R. Fässler. 2019. Integrin activation by talin, kindlin and mechanical forces. Nat. Cell Biol. 21:25–31. doi:10.1038/s41556-018-0234-9.

Theodosiou, M., M. Widmaier, R.T. Böttcher, E. Rognoni, M. Veelders, M. Bharadwaj, A. Lambacher, K. Austen, D.J. Müller, R. Zent, and R. Fässler. 2016. Kindlin-2 cooperates with talin to activate integrins and induces cell spreading by directly binding paxillin. eLife. 5:e10130. doi:10.7554/eLife.10130.

Tinevez, J.-Y., N. Perry, J. Schindelin, G.M. Hoopes, G.D. Reynolds, E. Laplantine, S.Y. Bednarek, S.L. Shorte, and K.W. Eliceiri. 2017. TrackMate: An open and extensible platform for single-particle tracking. Methods San Diego Calif. 115:80–90. doi:10.1016/j.ymeth.2016.09.016.

Tokuo, H., and M. Ikebe. 2004. Myosin X transports Mena/VASP to the tip of filopodia. Biochem. Biophys. Res. Commun. 319:214–220. doi:10.1016/j.bbrc.2004.04.167.

Watanabe, T.M., H. Tokuo, K. Gonda, H. Higuchi, and M. Ikebe. 2010. Myosin-X induces filopodia by multiple elongation mechanism. J. Biol. Chem. 285:19605–19614. doi:10.1074/jbc.M109.093864.

Wei, Z., J. Yan, Q. Lu, L. Pan, and M. Zhang. 2011. Cargo recognition mechanism of myosin X revealed by the structure of its tail MyTH4-FERM tandem in complex with the DCC P3 domain. Proc. Natl. Acad. Sci. U. S. A. 108:3572–3577. doi:10.1073/pnas.1016567108.

Wickham, H. 2016. ggplot2: Elegant Graphics for Data Analysis. 2nd ed. Springer International Publishing.

Young, L.E., C.J. Latario, and H.N. Higgs. 2018. Roles for Ena/VASP proteins in FMNL3-mediated filopodial assembly. J. Cell Sci. 131. doi:10.1242/jcs.220814.

Zhang, H., J.S. Berg, Z. Li, Y. Wang, P. Lång, A.D. Sousa, A. Bhaskar, R.E. Cheney, and S. Strömblad. 2004. Myosin-X provides a motor-based link between integrins and the cytoskeleton. Nat. Cell Biol. 6:523–531. doi:10.1038/ncb1136.

Zhu, L., J. Yang, T. Bromberger, A. Holly, F. Lu, H. Liu, K. Sun, S. Klapproth, J. Hirbawi, T.V. Byzova, E.F. Plow, M. Moser, and J. Qin. 2017. Structure of Rap1b bound to talin reveals a pathway for triggering integrin activation. Nat. Commun. 8:1–12. doi:10.1038/s41467-017-01822-8.
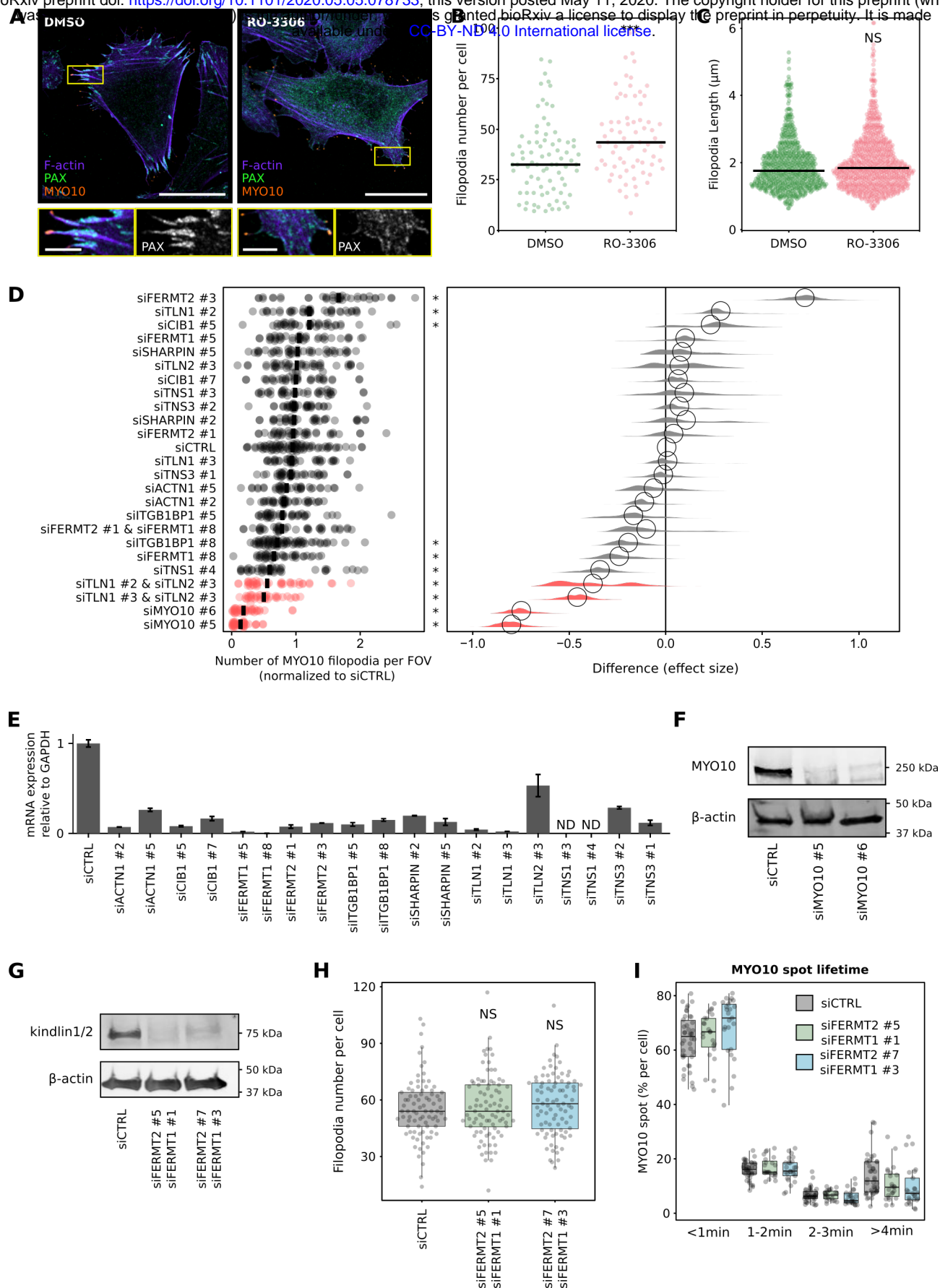
Fig. S1. Modulation of filopodia properties by focal adhesions and known integrin activity regulators. A-B) U2-OS cells expressing EGFP-MYO10 were plated on fibronectin for 1 h and treated for another hour with 10 µM RO-3306 (CDK1 inhibitor) or DMSO. Cells were stained for paxillin (PAX) and F-actin, and imaged using an Airyscan confocal microscope or a spinning disk confocal microscope. (**A**) Representative Airyscan images are displayed. The yellow rectangles highlight ROIs, which are magnified; scale bars: (main) 25 µm; (inset) 5 µm. (**B**) The number of MYO10-positive filopodia per cell was then quantified from the spinning disk images (n > 72 cells, two biological repeats; *** p-value = 0.003). **C**) Quantification of filopodia length, from SIM images, in U2-OS cells transiently expressing EGFP-MYO10 and treated for 1 h with 10 µM RO-3306 (CDK1 inhibitor) or DMSO (DMSO, n = 734 filopodia; RO-3306, n = 824 filopodia; three biological repeats; *** p-value = <0.001).

Fig. S1. (Continued from previous page.) **D-F**) RNAi screen of known integrin activity regulators. The indicated genes were silenced individually or together in U2-OS cells stably expressing EGFP-MYO10 using two independent siRNA oligos per gene. Cells were seeded on fibronectin-coated glass-bottom 96-well plates for 2 h and samples were fixed and stained. Samples were imaged using a spinning disk confocal microscope and the number of filopodia per field of view (FOV) was quantified automatically using ImageJ (see Methods for details). D) Results are displayed as dot plots. In addition, the effect size was calculated using bootstrapping to resample the median values for each of the conditions using PlotsOfDifferences (Goedhart, 2019). * p-value < 0.05. **E**) The efficiency of siRNA-mediated silencing of each target (except MYO10) was quantified by qPCR and normalised to GAPDH expression. The results were further normalised against expression detected in siCTRL cells. **F**) Efficiency of siRNA-mediated (oligos #5 and #6) silencing of MYO10 in U2-OS cells validated by western blot. **G**) Efficiency of dual siRNA-mediated silencing of FERMT1 and FERMT2 in U2-OS cells validated by western blot. **H**) FERMT1- and FERMT2-silenced U2-OS cells transiently expressing EGFP-MYO10 were plated on fibronectin for 2 h, fixed, and the number of MYO10-positive filopodia per cell was quantified (n > 70 cells, three biological repeats). **I**) FERMT1- and FERMT2-silenced U2-OS cells transiently expressing EGFP-MYO10 were plated on fibronectin and imaged live using an Airyscan confocal microscope (1 picture every 5 s over 20 min). For each condition, MYO10-positive particles were automatically tracked, and MYO10 spot lifetime (calculated as a percentage of the total number of filopodia generated per cell) was plotted and displayed as boxplots (see Methods for details; three biological repeats, more than 21 cells per condition). For all panels, p-values were determined using a randomization test. NS indicates no statistical difference between the mean values of the highlighted condition and the control.
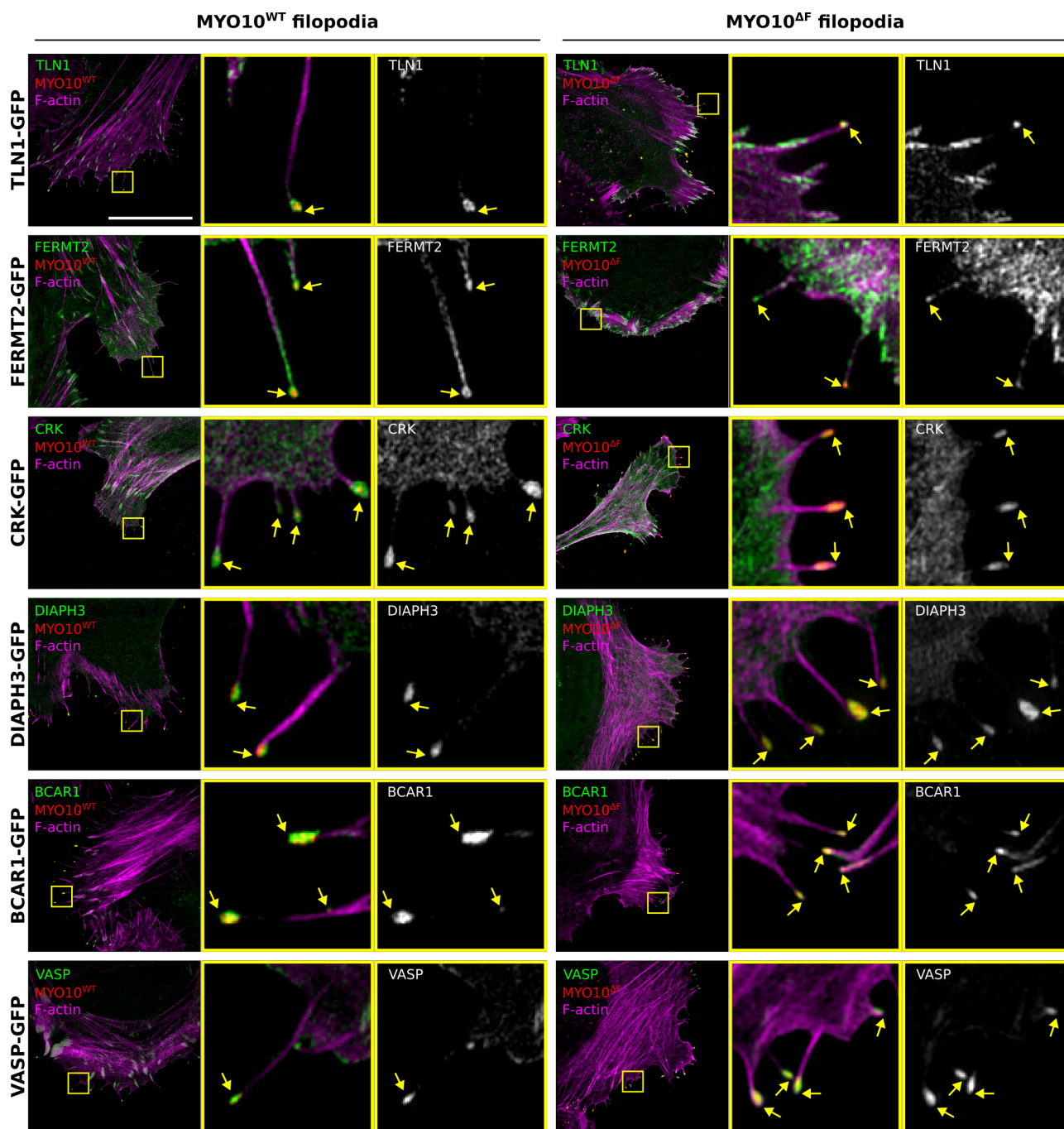
Fig. S2. MYO10 FERM deletion has minimal impact on filopodia tip protein localisation. U2-OS cells expressing MYO10^{WT}-mScarlet or MYO10$^{\Delta F}$-mScarlet-I together with TLN1-GFP, FERMT2-GFP, CRK-GFP, DIAPH3-GFP, BCAR1-GFP or VASP-GFP were plated on fibronectin for 2 h, fixed, stained for F-actin and imaged using SIM. Representative MIPs are displayed. The yellow squares highlight ROIs, which are magnified; yellow arrows highlight filopodia tips; scale bars: (main) 20 μm; (inset) 2 μm.
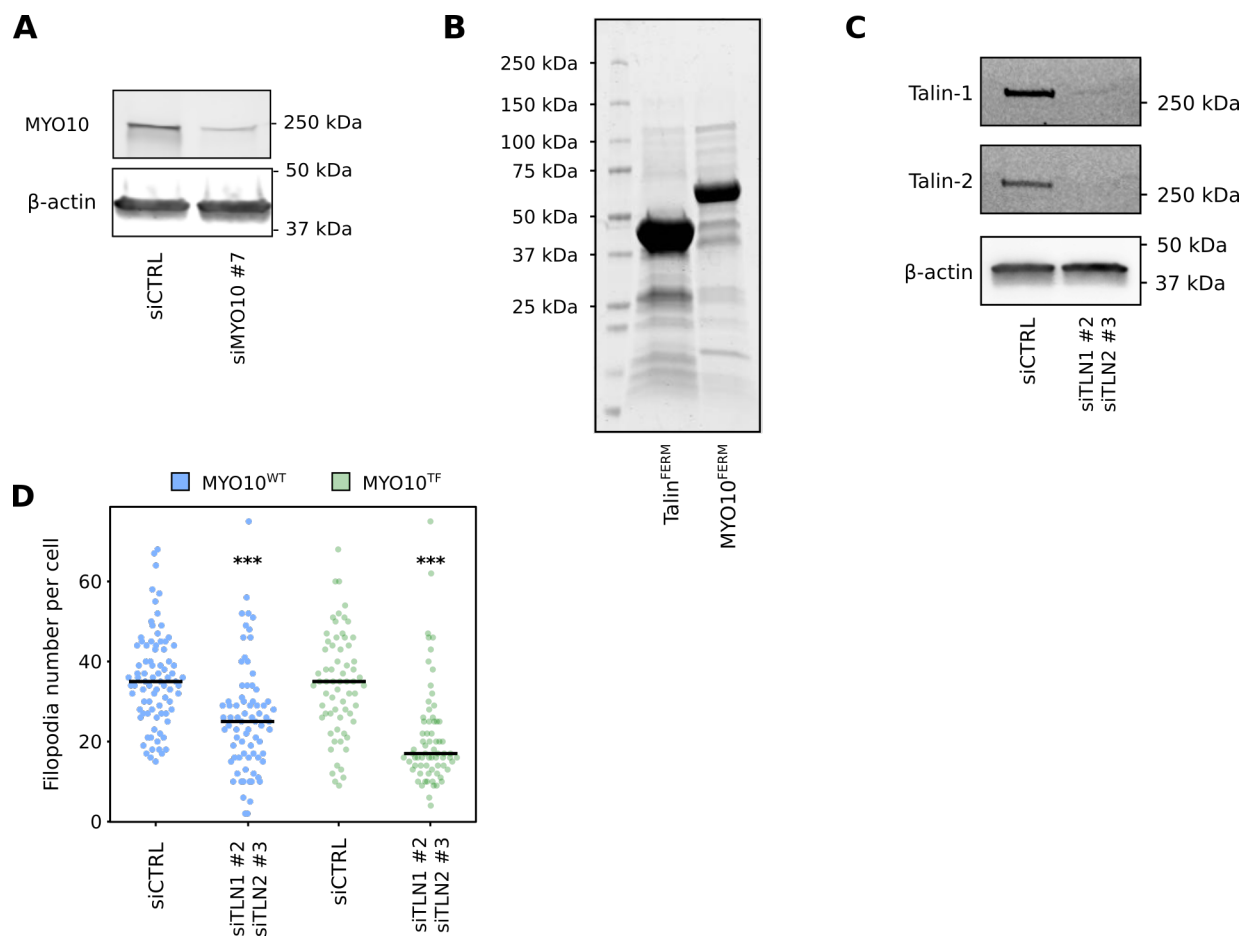
Fig. S3. Validation of MYO10 and TLN1/2 reagents. A) The efficiency of siRNA-mediated silencing of MYO10 in U2-OS cells was validated by western blot. The siMYO10 #7 oligo targets the 3' UTR of the MYO10 mRNA. **B**) Recombinant his-tagged TLN1 and MYO10 FERM domains were produced in bacteria and subsequently purified using a gravity Ni^{2+} column. A representative gel stained with Instant blue is displayed. **C**) Efficiency of dual siRNA-mediated silencing of TLN1 and TLN2 in U2-OS cells. A representative western blot is displayed. **D**) TLN1 and TLN2-silenced U2-OS cells transiently expressing EGFP-MYO10^{WT} or EGFP-MYO10^{TF} were plated on fibronectin for 2 h, fixed, stained, imaged using a spinning-disk confocal microscope, and the number of MYO10-positive filopodia per cell was quantified (siCTRL/MYO10^{WT}, n = 83 cells; siCTRL/MYO10^{TF}, n = 66 cells; siTLN1 and siTLN2/MYO10^{WT}, n = 75 cells; siTLN/MYO10^{TF}, n = 71 cells; three biological repeats, *** p-value < 0.001).